Universidade do Minho
Escola de Ciências

Pedro Manuel Lima da Silva

Bionanostructures for intracellular temperature sensing during hyperthermia cancer treatments

October 2018

Bionanostructures for intracellular temperature sensing during hyperthermia cancer treatments
Pedro Manuel Lima da Silva
UMinho | 2018

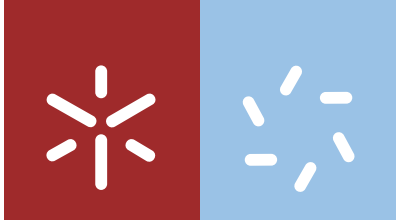

Universidade do Minho
Escola de Ciências

Pedro Manuel Lima da Silva

Bionanostructures for intracellular temperature sensing during hyperthermia cancer treatments

Master thesis
Master in Biophysics and Bionanosystems

Work developed under supervision of
Dr. rer. nat. Jana B. Nieder
INL – International Iberian Nanotechnology Laboratory

Prof. Dr. Maria Elisabete da Cunha Dias Real Oliveira
Universidade do Minho

October 2018

DECLARATION

Name: Pedro Manuel Lima da Silva

Email: plpedrolima92@gmail.com

Phone: 911753735

ID n°: 14192006

Thesis title: Bionanostructures for intracellular temperature sensing during hyperthermia cancer treatments

Supervisors:

Dr. rer. nat. Jana B. Nieder

Prof. Dr. Maria Elisabete da Cunha Dias Real Oliveira

Conclusion year: 2018

Master course: Master in Biophysics and Bionanosystems

IN ACCORDANCE WITH CURRENT LEGISLATION, THE REPRODUCTION OF ANY PART OF THIS THESIS / WORK IS NOT PERMITTED

University of Minho, October 2018

Signature: Pedro Manuel Lima Silva

Acknowledgements

The work developed in the frame of my master thesis was only possible due to the help of several people, to whom I would like to thank:

To Prof. Dr. Maria Elisabete da Cunha Dias Real Oliveira, for making the bridge between University of Minho and INL – International Iberian Nanotechnology Laboratory, that allowed me to join INL.

To Dr. rer. nat. Jana B. Nieder, for providing me with all the resources needed for the completion of my experiments. For her advices, immense expertise and motivation during the experiments and writing of the thesis.

To Dr. Oleksandr Savchuk, for supervision and closely following the development of the master project. For all the knowledge, brainstorming, advices and motivation provided.

To Dr. Oscar Silvestre, for all the knowledge and help in cellular behavior and cellular assays. To Ricardo Adão, for MATLAB expertise that allowed easier and accurate data analysis. To Dr. Edite Figueiras, for the knowledge in LABVIEW programing.

To all Ultrafast Bio- and Nanophotonics group members, for making me feel as part of the group, for the great work environment and availability to help when needed.

To Dr. Manuel Bañobre, for the collaboration of the Nanomedicine group in the project. For lending the AMF equipment, that without it this project would not be possible. To Dr. Juan Gallo, for the synthesis and knowledge of the magnetic nanoparticles used in magnetic hyperthermia experiments. To Dr. Lorena Hevia, for all the expertise in TEM sample preparation.

To my family for all the love, support and motivation throughout all my study period, that made it easier and allowed me to come this far.

To all my friends, for all the friendship, motivational words and all the moments that allowed me to relax and be absent from work.

Abstract

Cancer is a disease characterized by abnormal fast growth of cells. The current treatments used, chemo and radiotherapy, besides not being 100 % effective, have also serious side-effects. One of the most promising treatments under study are the hyperthermia ones, where a temperature increase is locally applied. One of such thermal treatments is magnetic hyperthermia, which is performed by local administration of magnetic nanoparticles and their exposure to an alternating magnetic field. This work aims at providing a method to assess the intracellular temperatures achieved during magnetic hyperthermia treatments.

The green fluorescence protein (GFP), that is compatible with live cells was used as a luminescent nanothermometer and can report temperature changes from various locations within the cell. Three different GFP variants were analyzed: i) nontagged-GFP was used to test temperature evolution in the cytoplasm, ii) Actin-GFP to test temperature along cytoskeleton proteins and iii) Mito GFP to test the local temperature at the mitochondria.

To assure nanothermal sensing during efficient magnetic hyperthermia treatment in *in vitro* live cell models, first the uptake of magnetic nanoparticles, their intracellular localization and toxicity were analyzed. Inductively couple plasma - optical emission spectroscopy (ICP-OES) results show that Fe_3O_4 nanoparticles are taken up in a concentration and time-dependent manner. A concentration dependent toxicity is observed at incubation times of 24h, with cell viability decreasing to values lower than 80 %, at concentrations higher than 50 μg/mL. Transmission electron microscopy (TEM) images reveal that such nanoparticles localize mainly in aggregates in vicinities of the nucleus membrane.

Temperature dependent studies showed a linear decrease of the GFP fluorescence lifetime with increasing temperature, while no correlation was observable with fluorescence polarization anisotropy when in actin-GFP proteins and in nontagged-GFP. Intracellular temperatures achieved during magnetic hyperthermia treatment using exposure times as reported for clinical tests, approximately 30 min, reach up to 75 °C degrees, which is considerably higher than required for the induction of local cell death.

In summary, a novel intracellular temperature measurement technique based on the fluorescence lifetime measurement of GFP was developed and validated within a range of magnetic nanoparticle concentration that is not considered toxic.

Keywords: Intracellular temperature, nanothermometer, magnetic hyperthermia, magnetic nanoparticles, fluorescence lifetime, fluorescence polarization anisotropy

Bionano-estrutruras para mapeamento da temperatura intracelular durante tratamento de cancro por hipertermia.

Resumo

O cancro é uma doença caracterizada por uma divisão celular anormalmente rápida. Os tratamentos convencionais usados (ex: quimio e radioterapia), além de não serem 100 % eficazes, possuem também sérios efeitos secundários. Atualmente os tratamentos hipertérmicos, são muito promissores, onde temperaturas acima do ideal são localmente aplicadas. A hipertermia magnética é um tipo de tratamento hipertérmico que consiste na administração local de nanopartículas magnéticas que são expostas a um campo magnético alternado.

Este trabalho teve como objetivo providenciar um método para detetar as temperaturas intracelulares atingidas durante este tipo de tratamento. A proteína verde fluorescente (GFP) foi testada como um nanotermómetro luminescente, para reportar diferenças de temperatura em vários locais intracelulares, uma vez que é compatível com células vivas. Foram analisadas três variantes de GFP: i) GFP não marcada para testar a evolução da temperatura no citoplasma, ii) actina-GFP para testar a temperatura no citoesqueleto, iii) mito-GFP para testar a temperatura na mitocôndria.

Para assegurar uma deteção eficiente das temperaturas atingidas durante a hipertermia magnética em modelos *in vitro*, foi analisado a internalização, localização intracelular e toxicidade das nanopartículas magnéticas. Os resultados de espectrometria de Emissão Ótica por Plasma Acoplado Indutivamente (ICP-ES) mostraram que nanopartículas de Fe_3O_4 foram internalizadas numa forma dependente do tempo e da concentração. Foi também observado que para tempos de incubação de 24 h, a toxicidade era dependente da concentração, apresentando uma viabilidade celular menor que 80 % para concentrações superiores a 50 μg/mL. Imagens de microscopia eletrónica de transmissão revelaram que estas nanopartículas se encontravam localizadas maioritariamente em agregados nas vizinhanças do núcleo.

Estudos dependentes da temperatura mostraram que havia uma diminuição linear dos tempos de vida de fluorescência com o aumento da temperatura, enquanto que não foi observada qualquer correlação na anisotropia de fluorescência polarizada quando se utilizaram células não marcadas ou marcadas com actina.

Durante o tratamento de hipertermia magnética, usando tempos de exposição comparados como os reportados em ensaios clínicos, foram atingidas temperaturas intracelulares de 75 °C, consideravelmente mais elevadas do que as temperaturas requeridas para induzir morte celular localizada.

Em resumo, foi desenvolvida e validada uma nova técnica de medição de temperatura intracelular baseada nas medidas de tempos de vida de fluorescência numa gama de concentrações consideradas não tóxicas.

Palavras-chave: temperatura intracelular, nanotermomêtro, hipertermia magnética, nanopartículas magnéticas, tempos de vida de fluorescência, anisotropia de fluorescência polarizada.

Contents

Table of abbreviations XI

Table of figures XIII

Chapter I – Introduction 1

1.1. Motivation 1

1.2. State of the art 2

1.3. Objectives and Goals 5

Chapter II – Theoretical background 7

2.1. Magnetic hyperthermia 7

2.2. Physical principles 12

2.3. Experimental techniques 19

Chapter III – Materials and methods 25

3.1. Magnetic nanoparticles synthesis 25

3.2. Cell culture 25

3.3. Uptake and toxicity assays 26

3.4. Sample preparation and nanothermometry studies 29

Chapter IV – Results and discussion 33

4.1. Implementation and optimization of an FPA mode in the a FLIM setup 33

4.2. Characterization of the interaction of cells with MNPs 35

4.3. Nontagged-GFP for intracellular temperature sensing during hyperthermia cancer treatments 41

4.4. Actin-GFP for intracellular temperature sensing during hyperthermia cancer treatments 51

4.5. Mitochondria-GPP for intracellular temperature sensing during hyperthermia cancer treatments 61

4.6. Comparison of GFP based fluorescence labels as nanothermometers 69

Chapter V – Conclusions and future perspectives 75

Chapter VI - References 77

Table of abbreviations

AMF - Alternating Magnetic Field 1
DMEM - Dulbecco Dulbecco's Modified Eagle's Medium 25
dSTORM - direct Stochastic Optical Reconstruction Microscopy 21
FPA - Fluorescence Polarization Anisotropy 4
GFP - Green Fluorescent Protein 2
Homo-FRET - Homo-Förster Resonance Energy Transfer 58
ICP-OES - Inductively Couple Plasma – Optical Emission Spectroscopy 19
IRF - Instrument Response Time 16
MNPs - Magnetic NanoParticles 1
NA - Numerical Aperture 21
PBS - Phosphate Buffer Saline 25
ROI - Region Of Interest 44
SAR - Specific Absorption Rate 10
STED - STimulated Emission Depletion 21
TCSPC - Time-Correlated Single Photon Counting 3
TEM - Transmission Electron Microscopy 20

Table of figures

Figure 2.1 – Representation of the hysteresis loop of both ferromagnetic and superparamagnetic materials. 9

Figure 2.2 - Representation of a Jabłoński's diagram. S_0 being the ground state and S_1 the first excited state. Absorption of a photon takes an electron to S_1 (blue arrows), that can lose energy by vibrational rotation (orange arrow) and through the release of a photon (yellow arrows). 13

Figure 2.3 – A) Representation of the 3D molecular structure of the green fluorescence protein designed with Pymol software, where a barel structure encases the fluorophore. B) GFPs absorption (blue line) spectrum between 300 nm and 530 nm with maximum excitation at 488 nm, and emission (green line) and an emission spectrum is between 470 and 650 nm. 14

Figure 2.4 – Representation of an exponential fit. The fluorescence lifetime values are obtained from the when the population of excited fluorophores decays to 1/e. 16

Figure 2.5 – Representation of the FPA working principle. 1) vertically polarized excitation leads to molecular photoselection; 2) vertically polarized emission by photoselected molecules; 3) vertical and horizontal emission after molecular rotation. 18

Figure 2.6 – Confocal microscope working principle. The volume of the excitation light is reduced by going through a first pinhole and a second one before the detector ignores the emission from outside fthe focal plane, thus increasing the resolution. 22

Figure 2.7 – Representation of the TCSPC principle. A pulsed light source is used to excite the sample with at a fluorescence intensity that gives a high probability of detecting only one photon per pulse. The time diference between the ligh pulse and the arrival of a photon is then used to build a histogram that can be exponentially fitted to retrieve the fluorescence lifetime. Adapted from [65]. 23

Figure 3.1 – Representation of the multi-well plate used to perform concentration dependent MNPs toxicity assay. Wells highlighted with dark and light grey were platted with a $5 * 10^4$ cells/mL cell density. Light grey wells were incubated in with different Fe_3O_4 MNP concentration for 24h. 20 % of final volume of resazurin were added to dark and light grey wells. 100 µL of PBS were added to the white wells to avoid medium evaporation. 28

Figure 3.2 – Representation of the costum-built FLIM setup used for intracellular temperature measurements. A 467 nm picosend laser is guided by mirrors and a dichroic to a 0.4 NA 20x objective, that focused the laser beam in the sample and collected the fluorescence emission. This

was then guided through a pinhole, to reduce emission from outside focal plane, into a polarizing beam splitter, that splits fluorescence emission in vertical and horizontal polarization, before reaching two APDs. The signal from the APDs is read by SPC electronics that enable TCSP. The is scanned with a micro and a nanopositioner, recording data in each pixel, allowing to build images in real-time by LabView based software. 30
Figure 4.1 – Implementation of real-time FPA capabilities in the custom-built FLIM microscope. Fluorescence polarization anisotropy equation was implement in a program based in LabVIEW. Hist. parallel and Hist. perp, are the TCSPC decay curves of the parallel and perpendicular polarizations. Each curve is summed to obtain a fluorescence intensity value that is used to calculate FPA..... 34
Figure 4.2 – Design of a 3D adapter to connect the AMF incubator to the piezo controlled nanopositioner during AMF. This was implemented using Sketchup software and printed with an Witbox, BQ device..... 34
Figure 4.3 – Intracellular iron content of HeLa cells. Cells were incubated for different times, 4, 8 and 24 h with two different concentrations of Fe_3O_4 MNPs. Intracellular iron content was determined by ICP-ES. Incubation with 50 μg/mL is represented by blue bars, while red bars represent 100 μg/mL. Cells incubated with 100 μg/mL MNPs had approximately two times more iron than cells incubated with 50 μg/mL. 35
Figure 4.4 - Intracellular localization of Fe_3O_4 MNPs. Cells were incubated for 24 h with 200 μg/mL of MNPs, and localization determined by confocal and TEM imaging (move to the text). A) Confocal microscopy with 63x objective in transmission mode. B) Transmission electron microscopy. Both imaging techniques show nanoparticles agglomerated in the vicinities of the nucleus. Zoomed TEM image, demonstrates a single nanoparticles with 10.4 nm diameter. 36
Figure 4.5 – Resazurin cell viability assay. HeLa cells were incubated for 24h incubation with different concentrations of Fe_3O_4 MNP, after which resazurin, 0.05 mg/mL, was added in volume equal to 20 % of the final volume and fluorescence intensity measured with an excitation at 560 nm. The percentagem of viable cells decreases with increasing concentration of nanoparticles. At 100 μg/mL the there is less than 80 %. 37
Figure 4.6 – HeLa cell transfect with nontagged-GFP. The tranfection leads to the GFP to be expressed in nontagged way in all cellular compartments. 41
Figure 4.7 – Temperature dependent fluorescence studies. HeLa cell transfected with nontagged-GFP for 24 h after which 50 μg/mL were added and incubated overnight. Medium was removed

and replaced by fresh one with risen step to remove not taken MNPs. Imaging was performed with a custom-built FLIM setup with controlled temperature set externally by circulating water bath and read by optic fiber immersed in sample medium. Fluorescence intensity images - A) Increase for higher temperatures. Fluorescence polarization anisotropy images – B) High heterogeneity in different regions of the cell and no clear dependency on temperature. Fluorescence lifetime images - C) Heterogeneity inside same cell, although visible decrease for higher temperatures. D) TCSPC multi-exponential fit of center region pixel shows no different between 18 and 29 °C. E) TCSPC multi-exponential fit of periphery region has different slopes at 18 and 29 °C. 43
Figure 4.8 – FPA and fluorescence lifetime temperature dependency. Average and standard deviations of FPA and FLIM measured in single HeLa cell, labeled with nontagged-GFP and incubated with 50 μg/mL of Fe_3O_4 MNPs. Analysis was done in two separate regions and plotted with two different colors. Different regions were analyzed due to visible heterogeneity. A) FPA values do not follow a linear tendency. B) FLIM decreases linearly with increasing temperature. 44
Figure 4.9 – Magnetic hyperthermia treatment dependent fluorescence studies. HeLa cell transfected with nontagged-GFP for 24 h after which 50 μg/mL were added and incubated overnight. Medium was removed and replaced by fresh one with risen step to remove not taken MNPs. Imaging was performed with a custom-built FLIM setup with applied 20 mT magnetic field, 224.53 ± 20 KHz and controlled external temperature set to 15 °C. Fluorescence intensity images – A) Decreased when exposed to AMF. Fluorescence polarization anisotropy images – B) Higher homogeneity with AMF exposure. Decrease is seen with higher exposure times. Fluorescence lifetime images – C) More homogenous when exposed to AMF. Values decrease for higher treatment times. D) TCSPC multi-exponential of center region fit shows different slope at 0 and 44 min. E) TCSPC multi-exponential fit in periphery region has different slopes at 0 and 44 min. .. 46
Figure 4.10 - FPA and fluorescence lifetime AMF exposure dependency. Average and standard deviations of FPA and FLIM measured in single HeLa cell, labeled with nontagged-GFP and incubated with 50 μg/mL of Fe_3O_4 MNPs while under 20 mT magnetic field. Analysis was done in two separate regions and plotted with two different colors. Same regions as in controlled temperature studies were analyzed. Intracellular temperature was deduced in the different regions with the respective equations. A) FPA values decrease linearly with higher exposure times. B) Fluorescence lifetime in center region decrease with higher exposure times. C) Fluorescence lifetime in periphery region decrease with higher exposure times. Highest deduced intracellular temperature of approximately 70 °C. 47

Figure 4.11 – Deduced intracellular temperature images. Temperature was calculated in pixel with the equations obtained from fluorescence lifetime linear fit. Temperature increase in entire cell body, with special focus in the periphery region. 48
Figure 4.12 – HeLa cell transfect with actin-GFP. The transfection leads to the GFP to be expressed in a bound form to actin proteins. This protein can be found in a globular and free form r polimerized creatng filaments. 51
Figure 4.13 - Temperature dependent fluorescence studies. HeLa cell transfected with actin-GFP for 24 h after which 50 μg/mL were added and incubated overnight. Medium was removed and replaced by fresh one with risen step to remove not taken MNPs. Imaging was performed with a custom-built FLIM setup with controlled temperature set externally by circulating water bath and read by optic fiber immersed in sample medium. Fluorescence intensity images – A) Decrease with higher AMF exposure. Fluorescence polarization anisotropy images – B) Heterogeneity in different regions of the cell, no dependency on temperature is visible. Fluorescence lifetime images – C) Homogeneous values inside same cell, decrease can be seen for higher temperatures. D) TCSPC multi-exponential fit of has different slopes at 18 and 29 °C. 53
Figure 4.14 - FPA and fluorescence lifetime temperature dependency. Average and standard deviations of FPA and FLIM measured in single HeLa cell, labeled with actin-GFP and incubated with 50 μg/mL of Fe_3O_4 MNPs. A) FPA imaging does not follow a linear tendency. B) FLIM decreases linearly with increasing temperature. 54
Figure 4.15 - Magnetic hyperthermia treatment dependent fluorescence studies. HeLa cell transfected with actin-GFP for 24 h after which 50 μg/mL were added and incubated overnight. Medium was removed and replaced by fresh one with risen step to remove not taken MNPs. Imaging was performed with a custom-built FLIM setup with applied 20 mT magnetic field, 224.53 ± 20 KHz and controlled external temperature set to 15 °C. Fluorescence intensity images – A) Decrease when compared to imaging performed before AMF exposure. Fluorescence polarization anisotropy images – B) Remains heterogeneous, decrease is seen with higher exposure times. Fluorescence lifetime images – C) More heterogeneus values, decreases with higher treatment times. E) TCSPC multi-exponential fit has different slopes at 0 and 37 min. 56
Figure 4.16 - FPA and fluorescence lifetime AMF exposure dependency. Average and standard deviations of FPA and FLIM measured in single HeLa cell, labeled with nontagged-GFP and incubated with 50 μg/mL of Fe_3O_4 MNPs while under 20 mT magnetic field. Intracellular temperature was deduced the respective equation. A) FPA values decrease linearly with higher

exposure times. B) Fluorescence lifetime decrease at higher magnetic hyperthermia treatment exposure. Deduced intracellular temperature reached approximately 75 °C. 57
Figure 4.17 - Deduced intracellular temperature image. Temperature was calculated in pixel with the equation obtained from fluorescence lifetime linear fit. Temperature increase in entire cell body, with special focus in the periphery regions and some regions in the nucleus vicinities. 57
Figure 4.18 - HeLa cell transfect with mito-GFP. The tranfection leads to the GFP to be expressed in bound form to E1 alpha pyruvate dehydrogenase present in the mitochondrial matrix. 61
Figure 4.19 - Temperature dependent fluorescence studies. HeLa cell transfected with mito-GFP for 24 h after which 50 μg/mL were added and incubated overnight. Medium was removed and replaced by fresh one with risen step to remove not taken MNPs. Imaging was performed with a custom-built FLIM setup with controlled temperature set externally by circulating water bath and read by optic fiber immersed in sample medium. Fluorescence intensity images – A) No clear changes at different temperatures. Fluorescence polarization anisotropy images – B) Heterogeneity throughout entire cell with an increase FPA values at lower temperatures. Fluorescence lifetime images – C) Heterogeneity inside same cell, but a decrease is seen for higher temperatures. D) TCSPC multi-exponential fit has different slopes at 18 and 29 °C. 63
Figure 4.20 - FPA and fluorescence lifetime temperature dependency. Average and standard deviations of FPA and FLIM measured in single HeLa cell, labeled with mito-GFP and incubated with 50 μg/mL of Fe_3O_4 MNPs. A) FPA decrease linearly with increasing temperature. B) Fluorescence lifetime values decrease linearly with increasing temperature. 64
Figure 4.21 - Magnetic hyperthermia treatment dependent fluorescence studies. HeLa cell transfected with mito-GFP for 24 h after which 50 μg/mL were added and incubated overnight. Medium was removed and replaced by fresh one with risen step to remove not taken MNPs. Imaging was performed with a custom-built FLIM setup with applied 20 mT magnetic field, 224.53 ± 20 KHz with frequency of and controlled external temperature set to 15 °C. Fluorescence intensity images – A) No significative change at different temperatures. Fluorescence polarization anisotropy images – B) Homogeneity with decrease values at higher exposure times. Fluorescence lifetime images – C) More homogenous values decreasing at higher treatment times. D) TCSPC multi-exponential fit has different slopes at 0 and 44 min. 66
Figure 4.22 - FPA and fluorescence lifetime AMF exposure dependency. Average and standard deviations of FPA and FLIM measured in single HeLa cell, labeled with mito-GFP and incubated with 50 μg/mL of Fe_3O_4 MNPs while under 20 mT magnetic field. Intracellular temperature was

deduced the respective equation. A) FPA values while under AMF exposure decrease linearly with higher exposure times. B) Fluorescence lifetime decreases with increasing AMF exposure time. Intracellular temperature was not deduced due to different values at same external temperature as in controlled temperature experiments. 67
Figure 4.23 – Relative thermal sensitivities. Relative sensitivities were calculated from the fitted data of the measurements with controlled temperature. Two different sensitivities were calculated for nontagged-GFP due to heterogeneities, sensitivities increase upon temperature increase and the with highest sensitivity was achieved in the periphery region. Actin-GFP sensitivity also increases with temperature. Mito-GFP sensitivities were calculated for both FPA and FLIM, with the highest achieved in FLIM measurements..... 70

Chapter I – Introduction

1.1. Motivation

Cancer is a disease that is primarily characterized by an abnormally fast cellular growth [1]. Cancer cells could potentially migrate to other body locations, in a process called metastasis [2], creating more tumors, which makes it difficult to treat [3].

Due to lack of effective treatment, this disease has become a major health problem. According to the International Agency for Research on Cancer, in 2018 there is an expected incidence worldwide of more than 18 million cases and more than 9 million deaths, expecting an increase of these values in the next years, reaching almost 29 million and more than 16 million, respectively, in 2040 [4]. Research is conducted worldwide to improve the available treatments and create new ones, such as an inhibition of negative immune regulation, which has been the subject to the Nobel Prize in Physiology 2018 that was awarded to Dr. James P. Allison and Dr. Tasuku Honjo.

One approach that reached clinical trials are hyperthermal treatments. This type of treatment is promising because cancer cells are more vulnerable to increased temperatures than normal cells, either dying faster or making them weaker and therefore easier to kill with other treatments [5]. This happens due to the way that the blood vessels are arranged in the tumor areas and the highly acidic environment, that makes it more difficult to dissipate the heat [6]. Although, higher temperatures have more effects on cancer cells, normal cells are also affected thus localized therapies are the optimal treatment.

Nanotechnology has emerged as a promising tool in cancer treatment. One of the nanotechnology based therapeutic strategies involves magnetic nanoparticles (MNPs) that can be injected directly on the tumor region or functionalized for specific targeting. These nanoparticles are exposed to an alternating magnetic field (AMF) for local heat production, in a treatment called magnetic hyperthermia.

However, there are still unknown factors that must be answered before adopting a hyperthermia treatment, such as the temperature reached inside the cell during the magnetic hyperthermia treatment. This is one of the major questions, because the intracellular temperature in such thermal treatment should be high enough to cause damages to cancer cells but not to damage normal cells in the surrounding tissues.

The work developed in this study, aims at delivering a noninvasive technology to assess intracellular temperature during cancer cell magnetic hyperthermia treatment. The green fluorescent protein (GFP) was selected as a biocompatible and luminescent probe that can be expressed at specific cellular structures and serve as noninvasive nanothermometer based on its temperature dependent fluorescence properties.

1.2. State of the art

Cells are complex systems, with various intracellular processes that strongly depend on temperature. Alterations in the DNA can make cells undergo non-stop proliferation, and this way lead to cancer. Heat treatments, like magnetic hyperthermia are being intensively studied as new type of cancer treatment. The existing problem with these treatments is that in order not to damage normal cells, the intracellular temperature should not be much higher than 45 °C and there is still no research in this specific problem.

With the advances in the field of nanotechnology, the ability to determine temperature at the nanoscale as become an important tool. For this purpose, several techniques for nanothermometry have been explored, that can be classified as contact or non-contact.

For nanoscale temperature measurement, a microscale thermocouple can be added to the tip of an atomic force microscope, allowing at same time mapping of surface relief and temperature [7]–[9]. The drawback of this type of measurement is that it requires contact making them invasive, and therefore is not suitable for intracellular temperature as it would require to penetrate the cell membrane, disturbing the cellular environment and probably kill it. Moreover, this technology would not fulfill the requirements to be translated into the clinics to monitor the temperature raised *in vivo* during a magnetic hyperthermia treatment, rather standing out as a proof-of-concept methodology *in vitro*.

For this purpose, the best are the non-contact, that are based on the interaction of light with matter, optical properties, that can be either from the material in study or of an additional molecule that works as the nanothermometer [10]. These ones can be divided in luminescent and non-luminescent.

Those luminescent include infrared thermometry, thermoreflectance, Raman spectroscopy and luminescence. Infrared thermometry is determined by the emitted radiation and it is, based on the blackbody radiation spectral distribution. This is a well-known technique, which is commercially available, but still for intracellular temperature this is not the best solution, mainly due to the

required emissivity of the material and the fact that the measurement is only done at the surface [11]. Thermoreflectance imaging is being employed in the temperature sensing of integrated circuits due to high spatial and temporal resolution. Temperature measurements are based on the changes of refractive index of the material that changes linearly with changes in temperature [12], [13]. Also, Raman spectroscopy can be used to determine temperature, due to highly temperature dependence of the anti-Stokes intensity, and no dependence of the Stokes intensity, thus allowing temperature measurement through the ratio between the two intensities [14].

For intracellular temperature studies, which was the goal of this work, luminescence techniques are the most suitable ones, due to the localization of the nanothermometer in the intracellular environment without damaging or disturbing the cellular function. For this type of studies different measuring techniques and materials have been reported as reviewed in [15]–[19]. These techniques could be used to assess the temperature achieved by hyperthermia treatments.

S. Uchiyama et al. (2018), developed a cationic fluorescent nanogel thermometer that showed an uptake, in four different mammalian cells, of more than 90 %. Such fluorescent nanogel thermometer showed temperature dependence on both fluorescence intensity and fluorescence lifetime in solution [20].

In 2014, *Takei Y. et al.*, developed a ratiometric nanothermometer based on a polymeric particle with thermosensitive fluorophore, β-diketonate chelate europium (III) thenoyltrifluoroacetonate and the thermoinsensitive fluorophore, rhodamine 101, which was used as a self-reference. The ratiometric measurements they performed were independent of environmental condition and effect of unfocusing. They also successfully tracked heat production correlated with cytosolic Ca^{2+} concentration in HeLa cells [21].

Another interesting approach was done based on the quantum mechanical temperature-dependent spin associated with nitrogen vacancy color centers in nanodiamond. The thermal resolution using this method reach the mK order of magnitude, which is the highest ever achieved in luminescence nanothermometry. The authors claimed that the controlled subcellular temperature gradient could enable the accurate control of gene expression, real-time observations of non-equilibrium subcellular processes and heat production by the chemical interactions involving a few or single molecules [22].

Okabe et al. (2012), used a fluorescence polymer for intracellular temperature mapping, with fluorescence lifetime as temperature variable. The time-correlated single photon counting (TCSPC) system-based lifetime imaging they used, provided high accuracy and spatial resolution. With this

study, they were able to show that cells have areas with different temperatures, being the higher ones in the nucleus and around organelles involved in the metabolism [23].

In neural cells was also demonstrated the existence of different temperatures in different cellular regions. For this evaluation, the authors used quantum dots as nanothermometer, and observed that neurites have a lower temperature than the cell body. In order to explain this they proposed two hypotheses: i) the cell body is where the nucleus is present and it shows a higher temperature, which would increase the temperature in that area, ii) neurites have a higher surface area to volume than the cell body, which makes easier for this region to dissipate heat [24].

Fluorescence polarization anisotropy (FPA) can also be used to assess temperature at the nanoscale. *Donner et al. (2012)* demonstrated the temperature gradient, with changed temperature by resistive heating and recording the temperature of the chamber, in GFP transfected HeLa and U-87 MG cell lines. Cells were surrounded by gold nanorods and exposed to an infrared laser irradiation to generate the temperature increase, due to heat release through the gold nanorods. A spatial resolution of 300 nm and temperature accuracy of about 0.4 °C were achieved [25]. The same approach was demonstrated *in vivo* using multicellular organism C. elegans that were transfected with GFP attached to the glutamic acid decarboxylase, further proving the potentiality in biomedical application of this method [26].

For intracellular nanothermometry, organic dyes are most probably the more suited ones because they do not induce any toxicity to sample. Also, they are easy and fast to use as well as commercially available, making them accessible and therefore a good solution.

Nanothermometers can be compared by relative thermal sensitivity, which can be defined by the percentage of change on the measurement per degree and is calculated with Equation 1.1.

$$S_r = \frac{1}{\Delta} \cdot \frac{\partial \Delta}{\partial T} \qquad 1.1$$

Where Δ is the quenching of luminescence and T the temperature. With the organic dye, reaching a relative thermal sensitivity of 19.6 %. K^{-1}, according to *Brites et al. (2012)*. Fluorescence nanothermometers possesses also one of the best resolutions, with 10^{-1} μm spatial resolution, 10 μs temporal resolution and 10^{-2} °K [11].

1.3. Objectives and Goals

The goal of this research project is the development and implementation of a non-invasive fluorescence based nanothermosensor able to accurately measure the intracellular temperature during cancer magnetic hyperthermia treatment. Temperature dependent fluorescence measurements were performed in a custom-built setup, which required the implementation of a FPA setup in the laboratory.

To achieve this goal the following tasks were performed:

- Optimization of the custom-built microscope for real-time FPA imaging
- Maintaining a HeLa cell culture expressing GFP for imaging experiments
- Assessment of thermal sensing capability using FPA contrast
- Assessment of thermal sensing capability using Fluorescence lifetime contrast
- Application of the nanothemosensor during magnetic hyperthermia treatment using an *in vitro* model.

This work was performed in the “Ultrafast Bio- and Nanophotonics” group at INL – International Iberian Nanotechnology Laboratory, and it was integrated in the ongoing research on intracellular temperature characterization framed within the CCDR-N project: "Nanotechnology based functional solutions" (grant no.: NORTE-01-0145-FEDER-000019).

Chapter II – Theoretical background

2.1. Magnetic hyperthermia

Hyperthermia, from the greek "*hyper"*, meaning above, *therm,* from the Greek *"thermo",* that means heat, is a type of treatment in which the body is exposed to temperatures above the optimal one. The potential of heat in the fight against cancer was discover long time ago, and was used by Hippocrates, to treat breast cancer. Upon promising results, he stated *"That which drugs fail to cure, the scalpel can cure. That which the scalpel fails to cure, heat can cure. If heat cannot cure, it must be deemed incurable."*, showing his conviction on the benefits of using higher temperatures to cure diseases [27].

Although there are some hyperthermia modes of application available, like local, regional and whole-body hyperthermia, using microwaves or radiowaves [28]. These heating modalities alone have no effect on killing cancer cells, but they are used to make them more vulnerable to classic treatments, such as radio and/or chemotherapy. Although the results achieved when high temperature and other treatment are applied in conjunction are promising, the patients are subjected to two different treatments [5], [6], [29]. This may cause additional discomfort, without removing the side effects of the classical therapies.

With the advances in nanotechnology a new type of hyperthermia treatment has been the field of intense research, namely magnetic hyperthermia, which involves the use of locally administrated MNPs as heat effectors that get activated under the exposure of an alternating magnetic field [30]. These nanoparticles are cell internalized and allow the local temperature increase, thus not damaging the healthy tissue surrounding the tumor region.

2.1.1. Magnetic nanoparticles

MNPs possess special size-dependent properties that are fundamental to its use in biological systems, such as inherent low toxicity, high stability (avoiding particle aggregation and thus blood vessel clogging), and superparamagnetic behavior as some of the most crucial ones.

Materials that show magnetic properties, can be classified in different groups, including diamagnetic, paramagnetic and ferromagnetic, depending on how they interact with magnetic fields.

Diamagnetic materials have all the electrons paired, thus all magnetic moments annulled. This means that when a magnetic field is applied this type of materials will not have spins available to be attracted to the direction of magnetic field, instead they are even slightly repelled [31].

Opposed to these materials are the paramagnetic ones, that have at least one unpaired electron, and therefore possess a magnetic momentum. Under a magnetic field this unpaired electrons will partially align their spins parallel to the magnetic field, having this way a weak magnetization [31].

In the aforementioned magnetism, when the magnetic field is turned off, the magnetization disappears, which would be ideal for this application, but the magnetization is weak and therefore not very suitable.

Ferromagnetic materials are composed of multi-domain particles in bulk state. These domains are separated by walls, inside which the spins are oriented parallel to each other but not to the spins on the order domains. This characteristic makes that inside of each domain there is a spontaneous magnetization, but overall the material is not magnetized due the different orientation of spins on different other domains. Applying a magnetic field to this type of materials, makes the domains move and rearrange themselves, conferring this way a magnetism to all the material [32]. When the magnetic field is removed, some magnetization is retained, which can be seen in Figure 2.1, meaning that to remove completely the remnant magnetization a magnetic field in the opposite direction must be applied. The required field is called coercivity [33].

As the size decreases to the nanometer scale, the particles start being single-domain. The critical diameter of a magnetic nanoparticle to become single domain is given by:

$$R_{sd} = \frac{36\sqrt{AK}}{\mu_o M_s^2} \qquad 2.1$$

Where A is the exchange constant, K is the magnetic anisotropy and M_s the saturation magnetization [33]. The size at which nanoparticles enter in the single-domain regime is been reported to approximately 40 nm [34]. In the single domain regime but above a so-called critical size, approximately 20 nm for Fe_3O_4 MNPs [35], the nanoparticles still show ferromagnetic behavior, therefore after magnetic field exposure the material remains magnetized.

For their use in biologic systems, like the human body, to have magnetized MNPs after magnetic field exposure is not desirable, due to the possibility of formation of aggregates that can block blood vessels, and therefore cause problems to the patient. To avoid this, the particles must have a type of magnetism called superparamagnetism [30].

For single domain uniaxial particles, the energy barrier to moment reversal equation is given by:

$$\Delta E = KV \tag{2.2}$$

Where K is the magnetic anisotropy, which is constant in uniaxial forms, and V is the volume of particle. It is possible to note that the energy barrier is very dependent on the volume of the particle [36].

The relaxation time, in Equation 2.3, is directly proportional to the energy barrier.

$$\tau = \tau_0 \, exp\left(\frac{\Delta E}{k_B T}\right) \tag{2.3}$$

Where K_B is the Boltzmann constant and T is the temperature. So, for particles below the critical size, the energy barrier is so low that ΔE is similar to $K_B T$. It allows that the thermal energy of the environment is enough to demagnetize them instantaneously after the magnetic field is off, which is called superpara-magnetism [37], [38]. This is a critical characteristic because it allows for a faster magnetization of the particles, but also to have no remaining magnetization and therefore no coercivity after magnetic field removal, as shown in Figure 2.1. Where a ferromagnetic material needs a strong magnetic field to become magnetized, at which the magnetization is approximately the highest. Upon magnetic field removal some spins stay aligned, therefore a magnetic moment remains. To remove the magnetization a magnetic field of approximately equal strength must be applied in the opposite direction. Different behavior is observed in superparamagnetic materials, the ones used in magnetic hyperthermia treatments. This ones are magnetized instantly when a

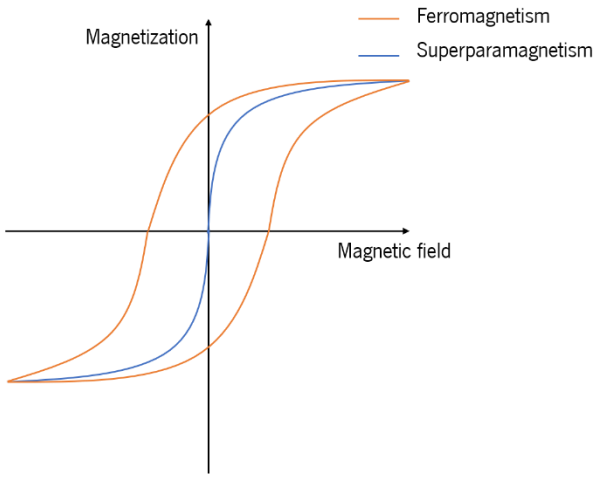

Figure 2.1 – Representation of the hysteresis loop of both ferromagnetic and superparamagnetic materials.

magnetic field is applied, and the spins become randomly oriented immediately after the magnetic field becomes zero, therefore no remaining magnetization is left.

Size, along with shape, composition and magnetic interaction and concentration, have also an important role in the heating properties of MNPs, namely specific absorption rate (SAR) [39]. This property is defined by the rate at which the nanoparticles absorb energy and is calculated by:

$$SAR = \frac{C\Delta T}{m * \Delta t} \qquad 2.4$$

Where C is the specific heat capacity of the medium, ΔT is the temperature change, m the mass of the sample and Δt the time interval. Therefore, is required that the particles have a high specific absorption rate to minimize the amount of MNPs used as well as the alternating magnetic field strength [40].

Besides the size, the coating of the particle is another aspect that is very important for the use in medical treatment [30]. Covering the nanoparticles with a coating avoids the deterioration of their physical properties, as well as making them stable in an aqueous solution.

To apply magnetic hyperthermia treatment, the MNPs are exposed to an alternating magnetic field. The relevance of the exposing the nanoparticles to this type of magnetic field is that the direction of the field changes with a certain frequency. Because magnetic moments of the particles align with the magnetic field, the orientation of magnetization changes with the same frequency.

There are two processes to which particles under a magnetic field release heat to the environment, that are also related with the size of the nanoparticle. These processes are Brownian and Néel's relaxation. Brownian relaxation relates to particle movement and rotation, therefore releasing heat from the friction with the solvent. Néel's relaxation is a process of spin rotation, that creates heat from the friction of the spins with inner crystal of the material. At nanoparticles with superparamagnetic properties, heat production is achieved by similar contributions of both mechanisms. Because the magnetic field is changing direction with the applied frequency, both the nanoparticles and their spins rotate with the same frequency to align parallel to the magnetic field, creating friction that promotes the heat release.

2.1.2. Clinical trials

Magnetic hyperthermia treatment has already been in clinical trials. In the first documented trial, conducted by *Johannsen M. (2010)*, it was applied to ten patients with diagnosed prostate cancer. Different volumes, 4-14 mL, of the magnetic fluid were injected through the perineum, under

general anesthesia. Although the equipment has possibility to generate magnetic field between, 3 and 18 mT, most of the treatment were kept between 5 and 6 mT. Higher magnetic fields were reported to cause discomfort to the patients. The temperatures were calculated through the iron mass, the computational tomography images and the specific absorption rate of the magnetic fluid and monitored directly during the treatment using invasive intraluminal thermometry in the urethra and anus. The maximum temperature achieved in the prostate was of 55 °C [41].

The second reported clinical trial, by *Matsubara T. (2013)*, was performed in six patients with bone cancer. This type of cancer is the cause of metastasis, which means that the patients have already little survival expectancy, and the surgery and other treatments are done to provide the patient more quality of life.

All patients received bone reconstruction with Fe_3O_4 nanoparticles and bone cement or calcium phosphate. The treatment was called electronic magnetic hyperthermia treatment and was performed ten times for 30 min each. The results showed that 80% of patients had bone union, and that all had pain relief and full functioning limbs [42].

The company, MagForce, received a European Certificate marking for MagTherm® treatment. This magnetic hyperthermia treatment is only applied to brain tumors, where a ferrofluid, NanoTherm®, is injected. The nanoparticles with average diameter of 15 nm, are then activated by an equipment composed of a 100 kHz coil, NanoActivator®. The size of the tumor is analyzed and the ferrofluid volume administrated accordingly. This approach is avoiding the exposure of normal cells to the heat released by the MNPs.

Although still making the first steps in the clinic, magnetic hyperthermia has been reported has a potential future treatment to cancer, as demonstrated by the acceptance for treatment of brain tumors. Before this can be fully implemented further studies must be made to prevent destruction of surrounding healthy tissues.

Temperature was reported in the surrounding tissues when treatment was applied, but the temperature inside the cells can be much higher than the ones reported in the clinical trials and therefore lead to damages that are not being considered yet, due to the lack of intracellular temperature study when such treatment is applied.

This work aimed to fill this gap and therefore study and provide knowledge on the temperatures reached inside the cells during magnetic hyperthermia treatment, hopefully helping it take a step forward.

2.2. Physical principles

2.2.1. Luminescence

Luminescence is the process of losing energy absorbed through the emission of photon. In 1933, Aleksandr Jabłoński, proposed a diagram where the processes of excitation and emission are explained [43]. Although there are now a huge number of adaptations of the initial diagram, it is always referred to as Jabłoński's diagram, shown in Figure 2.2. It represents the transitions an electron can undergo when gaining and losing energy.

The electrons in an atom have several energy levels at which they can be, being the ground electronic state the lower energy level, S_0. All molecules absorb energy, that can either be chemical, thermal or radiative, etc. If the electromagnetic energy transferred to molecules is high enough it can go to an excited state, S_1, in a process called absorption. The energy gained can be represented by Equation 2.5.

$$E=h\nu=\frac{hc}{\lambda} \qquad 2.5$$

Where, h is the Planck's constant, v is the frequency of the light, c is the velocity of light in vacuum and λ is the wavelength [44].

Staying in the excited states is not energetically favorable, and therefore the molecules lose energy through various processes. Vibrational relaxation occurs between the vibrational levels of the same electronic state. This process releases energy through non-radiative processes [45].

Fluorescence, is a process of losing energy with the release of a photon and it always happens from the lowest vibrational level of the excited state S_1 to all the vibrational levels of the ground electronic state, S_0 [45].

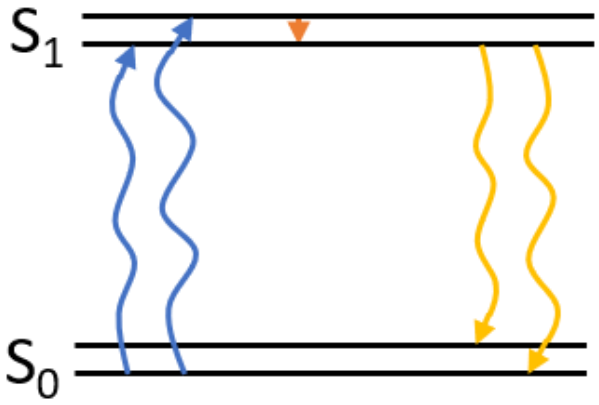

Figure 2.2 - Representation of a Jabłoński's diagram. S_0 being the ground state and S_1 the first excited state. Absorption of a photon takes an electron to S_1 (blue arrows), that can lose energy by vibrational rotation (orange arrow) and through the release of a photon (yellow arrows).

The term, fluorescence, was first used by Stokes, that proposed it to replace the term, dispersive reflection [46]. It was also Stokes through his studies on quinine, who observed it would only fluorescence when UV light was used and concluded that the emission wavelength is always higher than the absorption one. This phenomenon is known as Stokes' Shift [47].

The capability of emitting light is a very important property of some molecules that can be used for research purposes, since fluorescence allows to perform various types of studies, through parameters like fluorescence intensity, fluorescent polarization anisotropy (FPA) and fluorescence lifetime measurements. Changes in these properties induced by exposure to different environment conditions, give knowledge on the changes that are occurring. For instance, in biological samples, it is very useful to have information on microenvironment conditions, such as the pH, viscosity and temperature. Many molecules of different characteristics can be used, although, if possible, the organic probes are the best ones for this purpose, due to not having toxicity to cells.

The green fluorescence protein (GFP) molecular structure, designed with Pymol software, can be seen in Figure 2.3 A. This protein was first isolated in 1962, was by Dr. Osamu Shimomura, work for which he was granted a Nobel Award in 2008, along with Dr. Martin Chalfie, that demonstrated the value of GFP in cellular research purposes, and Dr. Roger Y. Tsien, that contributed with the knowledge of GFP fluorescence and also came up with proteins of different colors, allowing this way for different studies simultaneously in same cells [48]. Since then this protein has been widely used in studies of intracellular phenomena.

In Figure 2.3 B, characteristic spectra of enhanced green fluorescent protein (eGFP) can be seen, the excitation occurs mostly in the blue zone of the visible spectrum, with an excitation spectrum between the 300 nm and 530 nm with maximum excitation at 488 nm, and a fluorescence emission spectrum in between 470 and 650 nm.

GFP is a protein that has become a very useful tool for research and made a revolution in intracellular studies, due to the possibility of attaching it to other molecules of interest, that can be done in two different ways. It can be transfected to the cell, that is done by the insertion of the genetic material encoding to GFP, in a way that the cell starts to express it. This is very useful to gene expression research, since it allows to express the GFP attached to the protein of interest, and this way being possible to follow them [49]. Or they can be attached to some molecule outside the cell, to perform uptake studies [50].

These two approaches give the possibility to perform many studies, by reporting on the environment or interactions that happen inside the cells. For instance, it can give information on interactions between proteins, the position inside the cell. Furthermore, it can provide information on pH, viscosity, polarity and temperature [25], [51], [52].

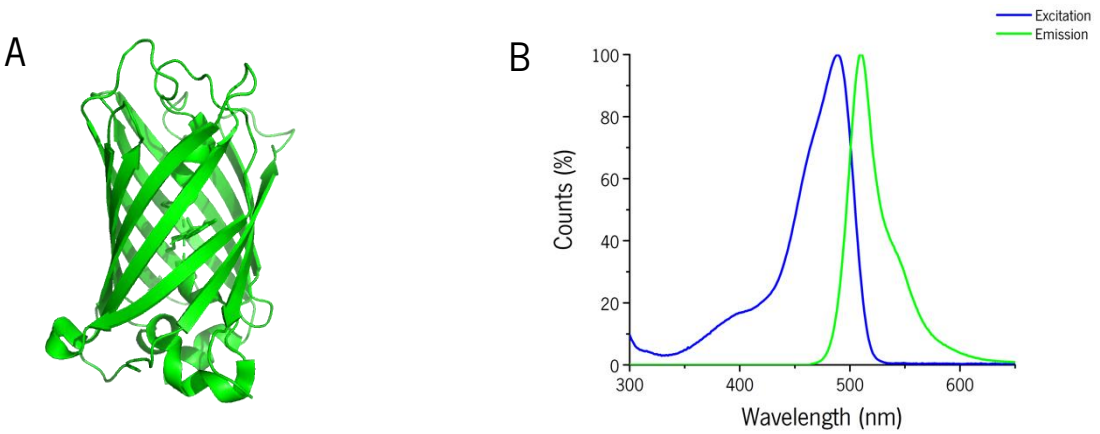

Figure 2.3 – A) Representation of the 3D molecular structure of the green fluorescence protein designed with Pymol software, where a barel structure encases the fluorophore. B) GFPs absorption (blue line) spectrum between 300 nm and 530 nm with maximum excitation at 488 nm, and emission (green line) and an emission spectrum is between 470 and 650 nm.

2.2.2. Fluorescence Lifetime

Excitation by pulsed light source promotes a non-stationary density of centers N in the excited state. These excited centers can decay to the ground state by radiative and non-radiative processes providing with relevant information on kinetics behavior. The kinetic evolution of the excited state population follows a general rule:

$$\frac{dN(t)}{dt} = -A_T N(t) \qquad 2.6$$

where A_T is the total decay rate, which can be written:

$$A_T = A + A_{nr} \qquad 2.7$$

Where A is the radiative rate and A_{nr} is the nonradiative rate. By solving differential Equation 2.6, density of excited centers at time t is following:

$$N(t) = N_0 e^{-A_T t} \qquad 2.8$$

where N_0 is the density if the excited centers at time equal zero, just after a pulse of light has been absorbed. Since emitted light intensity I_{em} at a given time t is proportional to the density of centers per time, it will result in:

$$I_{em}(t) = I_0 e^{-A_T t} \qquad 2.9$$

where, I_0 is the emitted intensity of light at time zero. Equation 2.10 describes exponential decay law for the emitted intensity of light and the lifetime is given by:

$$\tau = \frac{1}{A_T} \qquad 2.10$$

This lifetime is called fluorescence or luminescence lifetime and represents the time in which the emitted intensity of light decays to I_0/e. It can be obtained from the slope the linear plot log I versus t or by fitting the decay curve to an exponential Equation. According to Equation 2.11, this lifetime value gives the total decay rate (radiative and nonradiative) that can be written:

$$\frac{1}{\tau} = \frac{1}{\tau_0} + A_{nr} \qquad 2.11$$

Where τ_0 is radiative lifetime (time measured for purely radiative process).

As shown above in Jablonki's diagram, a molecule after promoting to the excited state, undergo several processes to return to the grown state.

Therefore, the molecules stay in the excited state for this time, that is called fluorescence lifetime, and is given by:

$$dN = (k_r + k_{nr})N(t)\,dt \qquad 2.12$$

Where N is the number of molecules in the excited state, and dN the number of molecules returning to the ground state after a certain time (t) [53].

This Equation can then derive in:

$$N = N_0 e^{-t/\tau} \qquad 2.13$$

In which N_0 is the number of molecules in the excited state at time zero.

From Equation 2.13 is then possible to see that fluorescence lifetime is the time required for the population of excited molecules to decrease to $1/e$ [54].

Experimental data acquired can be fitted to an exponential decay, Figure 2.4, and the fluorescence lifetime retrieved with a deconvolution of the instrument response time (IRF), that is the shortest fluorescence lifetime measured with the setup in use.

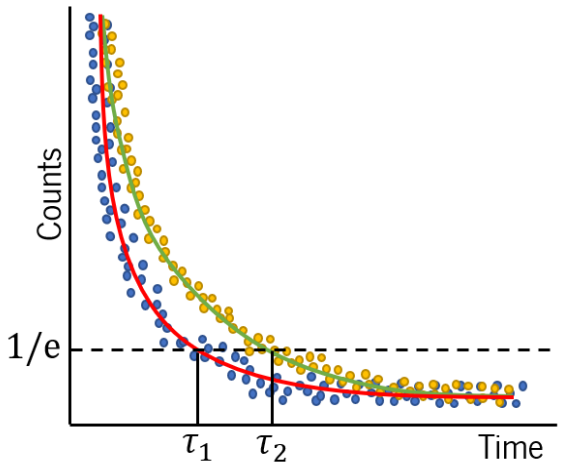

Figure 2.4 – Representation of an exponential fit. The fluorescence lifetime values are obtained from the when the population of excited fluorophores decays to $1/e$.

2.2.3. Fluorescence Polarization Anisotropy

Fluorescent polarization anisotropy relies in the orientation of the molecular dipole moments, and its working principle is represented in Figure 2.5.

For FPA studies, the excitation light must be polarized (1), since the probability of a molecule absorbing a photon and therefore going to an excited state is much higher when the fluorophores have the absorption transition moments oriented along the electrical vector of incident light [55]. The excitation of the fluorophores with the moments aligned parallel to the excitation source, leads to a key aspect in FPA, that are photoselected fluorophores.

The emission of this fluorophores is also polarized, with the same orientation of the excitation light, which means that the emission is parallel to the excitation (2). As molecules rotate, the dipole moments of the molecule also rotate, making that the molecules that were previously excited, emit in a different direction than the parallel, meaning perpendicular emission (3). This causes polarization to decrease, that leads to the fluorescence polarization anisotropy values to decrease [47]. The FPA is described on the amount of polarization and can be calculated using Equation 2.14 [56]:

$$FPA = \frac{I_{II} - GI_{\perp}}{I_{II} + 2GI_{\perp}} \qquad 2.14$$

Where $I_{\parallel}$ is value of the intensity of fluorescence that is polarized parallel to the incident light, the $I_{\perp}$ is the value of the intensity when the emission light is perpendicular [56], [57]. G is a correction factor of the instrument, accounting for the different sensitivities the detectors have for light with different polarization and can be determined, by measuring a sample with a known FPA value of approximately zero, which solving Equation 2.14, gives:

$$G = \frac{I_{II}}{I_{\perp}} \qquad 2.15$$

In the Equation 2.14 the denominator is the total intensity from the sample, the $I_{\perp}$ is multiplied by 2, because it represents the intensity of perpendicular light, that comes from two axis.

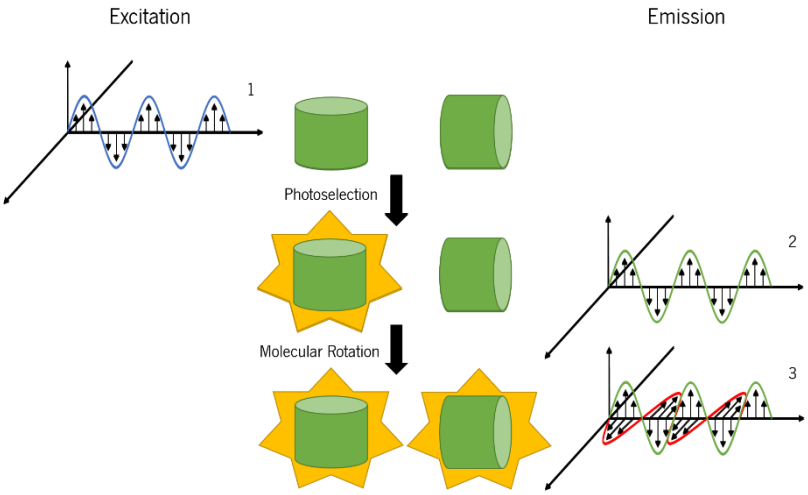

Figure 2.5 – Representation of the FPA working principle. 1) vertically polarized excitation leads to molecular photoselection; 2) vertically polarized emission by photoselected molecules; 3) vertical and horizontal emission after molecular rotation.

This technique is also used to determine the viscosity of the environment in which the molecule is present, due to the rotational movement of the molecule. If the environment is not so viscous the molecule will have more freedom to rotate, while if it is denser the molecule will be more stable and rotate less [58]. The relation of FPA with the molecular rotation caused by Brownian motion is described by Perrin Equation (Equation 2.16) [59]:

$$\frac{1}{FPA} = \frac{1}{FPA_0}\left(1 + \frac{\tau_F}{\tau_r}\right) \qquad 2.16$$

Where FPA_0 is the FPA value in the absence of rotation, τ_F is the fluorescence lifetime and τ_r is the rotational correlation time. When the temperature increases, the Brownian motion is accelerated and hence the molecules will rotate much faster. The more the molecule rotate during their fluorescence lifetime the more emitted photons will have polarization different from excitation one. Thus, temperature increase leads to a decrease of polarization of the fluorescence. Debye-Stokes-Einstein equation describes relation between temperature and rotational correlation time [57].

$$\tau_r = \frac{V\eta}{k_B T} \qquad 2.17$$

Where V is the hydrodynamic volume of the molecule, η is the viscosity of the environment, k_B is the Boltzmann constant and T is the temperature.

If a molecule has a much lower rotational correlation time (τ_r) than fluorescence lifetime (τ_F), the molecule rotates faster during the fluorescence lifetime, which leads to a total depolarization and therefore no changes at different temperatures can noticed. On other hand, if the τ_r is orders of magnitude higher than τ_F, then the molecule does not rotate enough during its fluorescence lifetime which leads to the polarization being too high.

To achieve values of FPA that show changes with different temperatures, the rotational correlation time and fluorescence lifetime must be of the same magnitude order.

From Equation 2.17 hydrodynamic volume and viscosity are the crucial parameters to be modified, to increase the sensitivity of the technique. Viscosity can be increased by using glycerol-water mixture, although it is not recommended for biological studies due to the cytotoxicity of the glycerol [25]. So, selecting a molecule with a hydrodynamic volume that gives a τ_r value of interest is the key factor to obtain more sensitive FPA.

Temperature measurements by FPA where reported before by *Donner et al. (2012)*. In their studies they used HeLa and U-87 MG with a GFP expressed freely in the entire overall cell [25].

2.3. Experimental techniques

2.3.1. Inductively couple plasma – Optical Emission spectroscopy

Inductively couple plasma - optical emission spectroscopy (ICP-OES) is a technique for the determination of the components on a sample, as well as their concentration.

It consists on argon gas flowing in a chamber, a spark ionizes argon atoms and starts a plasma. The argon ions are then accelerated by a radio-frequency coil at high frequency and collide with other argon atoms, transferring energy and therefore removing electrons from them as well. As long as the radio-frequency is on the argon atoms keep being ionized and therefore plasma continues active, the argons ions continuously ionize other argon molecules, thus the name inductively couple plasma.

The sample passing through is them sprayed in the form of droplets in the beginning of the plasma. Because the temperature of the plasma is so high, reaching up to 10^4 °K, the solvent in which the sample is dissolved immediately evaporates, and the sample that reaches the plasma is therefore in the solid state. This is them evaporated and reduced into the atoms that constitutes the sample. The atoms are then ionized and excited, therefore emitting radiation that is detected by a

photomultiplier tube. First samples with known concentration are used to build a calibration curve [60].

2.3.2. Transmission electron microscopy

Transmission electron microscopy (TEM), is a microscopy technique that uses electrons instead of light as energy source. It was first created in 1933 by Prof. Ernst Ruska, work for which he was award a Nobel Prize in Physics [61].

In order to release electrons from atoms, the energy given to them needs to be equal or higher to the attraction forces between the atoms used. The most commonly used sources are a tungsten filament or crystal of lanthanum hexaboride, due to low energy required to release electrons. These are then shot in a vacuum chamber that as negative potential to accelerate the electrons. The electron beam is then focused by an electrostatic lens, and them usually two condenser lenses that focus the electron beam to the sample. Electrons that are transmitted through the specimen are collected and focused by an objective and magnified in a phosphorescent screen to visualize the image [62].

The resolution on the images collected with this microscopy can be much higher than in optical microscopes, due the shorter wavelength of electron beam compared with light sources [63].

In cellular studies, to avoid deformations and see the various cell membranes, the samples preparations must be dried, stained and solidified [63].

With the research in nanoparticles for the administration in cells, this microscopy technique has been used to determine if the particles are inside the cell [64]–[66].

2.3.3. Cell viability

Cell viability studies assess how healthy the cells are by measuring the number of live or dead cells in a total cell sample. There are several studies that can be done, such as the MTT (3-(4,5-dimethylthiazol-2-yl)-2,5-diphenyltetrazolium bromide) assay, that relies in the metabolization of MTT into formazan, that as purple color. The measurements are than performed by absorbance with a light source around 560 nm [67]. DLH, is also a cell viability assay, based on the formation of formazan. The difference to the MTT is that the formazan is the product of the interaction of pyruvate, from the enzymatic reaction of the lactate dehydrogenase, with iodonitrotetrazolium chloride. The concentration of formazan in the cell culture medium is then directly related with membrane rupture, and therefore cell death [68].

Resazurin (7-Hydroxy-3*H*-phenoxazin-3-one 10-oxide) is a molecule that by itself, has blue color, but no fluorescence. When this is added to a cell sample, metabolic active cells reduce the molecule to resorufin that has red color and strong fluorescent signal, with an excitation spectrum from 400 to 600 nm and emission spectrum ranging from 450 to 600 nm.

Because only the live and metabolic active cells can reduce the molecule, this is a very useful, simple and reliable assay to assess the percentage of live cells, and therefore the toxicity effect in study [69].

Amongst the options stated resazurin proves to be one of the best due to not being expensive and also more sensitive than the MTT assay [67].

2.3.4. Confocal microscopy

In cellular studies, microscopy studies are a standard and widely used technique because it enables imaging the cells and therefore a more visual stimulus which provides better understanding in a more appealing way. Nowadays there are several fluorescence microscopy techniques, such as epifluorescence microscopy and super resolution microscopy, like stimulated emission depletion (STED) and direct stochastic optical reconstruction microscopy (dSTORM). These techniques take advantage of fluorescent molecules to study intracellular processes at specific organelles and can offer higher resolution than the optical microscope. Another of this, is the inverted confocal microscope, that is now present in most imaging laboratories, due to the higher resolution that it provides. In Figure 2.6 a representation of the working principle of a confocal microscope is shown. A light source, usually a laser, passes through a pinhole before being directed to the sample by a dichroic mirror. The laser is then focused in the sample by a high numerical aperture (NA) objective, allowing the fluorophores to go to an excited state and therefore fluoresce.

The high NA objective is used to improve the microscope resolution, that is the smallest distance between two points to which they can be seen separately, and is given by:

$$r = \frac{\lambda}{2NA} \tag{2.18}$$

Where, λ is the wavelength. From the Equation 2.18 is possible to see that the higher the NA the lower the distance between points, and therefore the higher resolution. The resolution of a confocal

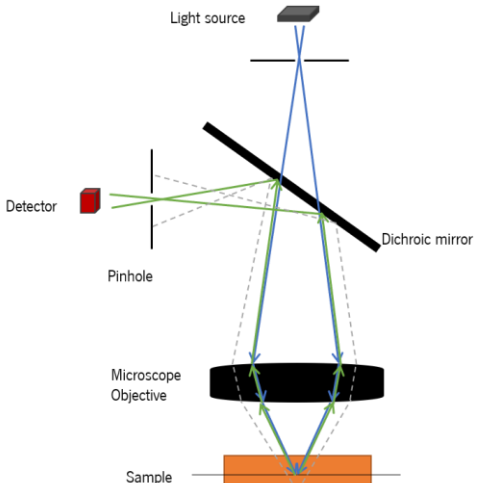

Figure 2.6 – Confocal microscope working principle. The volume of the excitation light is reduced by going through a first pinhole and a second one before the detector ignores the emission from outside fthe focal plane, thus increasing the resolution.

microscope is set by the diffraction-limit and thus dependent on the wavelength of the excitation source.

Fluorescence signal from the sample is collected with the same objective and after hitting the dichroic, which eliminates reflection of the laser, is focused in a pinhole before reaching the detectors. Through this pinhole passes the fluorescence light that was emitted from the focal plane in the sample and rejects all other light coming from different places in the sample. This allows for reduction of the background noise that would make the images blurrier, and therefore provide sharper and clear images.

2.3.5. Time-correlated single photon counting

Time-correlated single photon counting is a technique based in the repetitive and precisely timed detection of a photon emitted by a sample after being excited by a pulsed laser.

A high repetition laser is used to excite a sample that then emits light in the form of fluorescence. On Figure 2.7, the principle of TCSPC is represent. At each laser pulse a watch starts and stops at the arrival of a photon to the detector. The time elapsed from the excitation to the detection of a photon allows to build a time dependent photon arrival histogram with an exponential decay, e.g. in Figure 2.7 [70].

For optimized results, one should perform such technique with a fluorescence intensity low enough to assure that single photons are detected. Not doing so, the arrival of more than one photon, would lead to the registration of the first photon and therefore that the shorter times are more

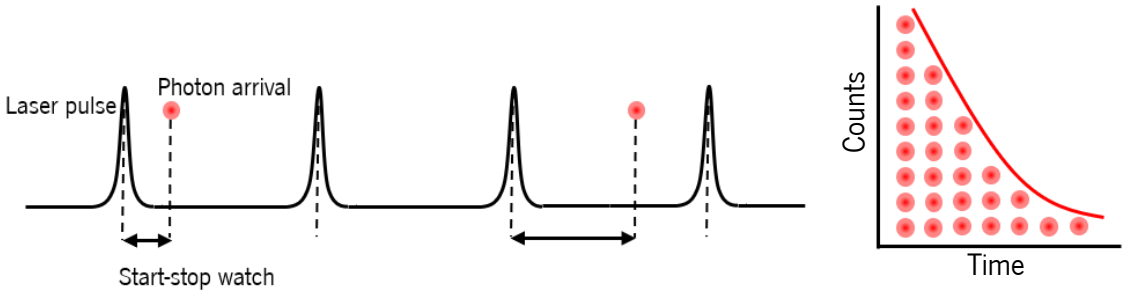

Figure 2.7 – Representation of the TCSPC principle. A pulsed light source is used to excite the sample with at a fluorescence intensity that gives a high probability of detecting only one photon per pulse. The time diference between the ligh pulse and the arrival of a photon is then used to build a histogram that can be exponentially fitted to retrieve the fluorescence lifetime. Adapted from [71].

represented, due to inability of the systems of processing the following photons, and therefore have shorter fluorescence lifetime values [71].

2.3.6. Fluorescence lifetime imaging microscopy

Fluorescence lifetime imaging microscopy is the conjugation of the TCSPC capabilities with a microscope.

The sample is scanned in a microscope, being the TCSPC data acquired in each pixel, giving an overall data in the form of a three-dimensional matrix, with the x-y coordinates and the histograms built from the TCSPC in each pixel [72].

Using a microscope, enables the possibility of creating a fluorescence lifetime image, which allows for high spatial resolution, given by a confocal microscope.

The advantages of using such technique is that the fluorescence lifetime is not dependent of external conditions, like photobleaching or optical alignment, which makes it very suitable to the studies of variations in the close environment. Moreover, it is also independent of scattering and effects of the background, making it a reliable feature [70].

These advantages make it a very interesting technique for biological studies [73]–[75].

2.3.7. Fluorescence polarization anisotropy imaging

Fluorescence polarization anisotropy imaging is built of an image with FPA values in each pixel.

Because the data is collected with two different detectors, with the fluorescence being split in two different polarizations by a polarizing beam splitter. The fluorescence intensities recorded are used

to calculate FPA values through the Equation 2.14 [76]. Combining this fluorescence parameter with a microscope allows for the retrieval of FPA with high resolution and therefore apply it to study and unveil intracellular processes. The advantages of this techniques is that it is not affected by changes in fluorescence intensity, and therefore insensitive to photobleaching.

Although higher resolution is interesting and very appealing, the use of objectives with higher NA may cause further depolarizations, and therefore give values that are not true [77].

The FPA imaging has already been used for some biology research, in temperature measurement and interaction between proteins [25], [78], [79].

Chapter III – Materials and methods

3.1. Magnetic nanoparticles synthesis

MNPs were provided by the INL – International Iberian Nanotechnology Laboratory, Nanomedicine group. The synthesis was performed under the following conditions.

Iron (II) chloride and iron (III) chloride were dissolved in 10 mL of milliQ water. In a separate vial, poly(acrylic acid sodium salt) was dissolved in 5 mL of milliQ water. Both solutions were mixed together in a PTFE reactor and 15 mL of concentrated (28-30%) ammonium hydroxide solution were added into the reactor. The PTFE reactor was closed with a PTFE lid and sealed in a general-purpose Parr autoclave reactor. The solution was hand shaken and the reactor was placed in an oven at 150 °C for 24h. After 1 day the autoclave was allowed to cool down to room temperature and the solution was diluted down with acetone and centrifuged at 8500 rpm for 5 min. The supernatant was discarded, and the pellet resuspended in 15 mL of milliQ water. This water solution was centrifuged at 3000 rpm for 3 min to remove large aggregates, the pellet was discarded, and the solution stored until further use in a glass vial.

The sample of magnetite nanoparticles in water was destabilized with acetone and centrifuged at 8500 rpm for 5min to get a pellet. The supernatant was discarded, and the pellet resuspended in water. This process was repeated twice. Finally, the pellet was resuspended in a known volume of milliQ water. The nanoparticles concentration was measured to be 1.984 mg/mL.

3.2. Cell culture

The research was conducted with the use of HeLa cells (Sigma), originally from a cervical cancer of Henrietta Lacks. These were the first cell line to be immortalized, and are therefore the most famous cell line available [80].

Cells were platted and grown in T75 flasks (ThermoFisher Scientific) with 10 mL cell culture medium, composed of Dulbecco Dulbecco's Modified Eagle's Medium (DMEM) from with 4.5 g/L glucose (Lonza) with additional 10 % Fetal Clone® III (GE Healthcare, US) and 1 % penicillin/streptomycin (SigmaAldrich). Medium replacement was performed twice per week, during which washing steps were done with 5 mL Phosphate Buffer Saline (PBS) (CORNING) and detached from the flask surface with 2 mL of trypsin-EDTA (Gibco®). All cell sample preparations were done under a laminar flow hood (Telstar – Bio II Advance).

3.3. Uptake and toxicity assays

This chapter describes the methods and materials used to assess the characterization of the interaction of MNPs with HeLa cells.

3.3.1. Sample preparation and ICP-OES measurements

The quantitative analysis of internalized Fe (Fe_3O_4 nanoparticles) was performed by ICP-OES measurements.

Cells were plated in T25 cell culture flasks, with a concentration of 3 * 10^5 cells/mL and let attach for 24 h. After, incubation was done at 37 °C, with two different concentrations of MNPs, 50 and 100 μg/mL, for three different time points, 4, 8, 24 h, to assess the optimal internalization. Cell detachment was performed by the addition and incubation for 5 min with 2 mL of trypsin-EDTA, after two times washing with the 5 mL of PBS. Cells were recovered into a 15 mL falcon tube, used to remove the trypsin-EDTA with a 5 min centrifugation at 1200 rpm.

Finally, the formed cell pellet was resuspended in 1 mL of 37 % HCl to digest the cell membrane and MNPs overnight, after which it was diluted with 7 mL of milliQ water.

The Fe concentration was determined by ICP-OES using an ICPE-9000 multitype ICP Emission Spectrometer from Shimadzu. Measurements were performed in triplicate, to allow standard deviation calculation.

3.3.2. Sample preparation and TEM imaging

TEM imaging was performed, to provide images of the intracellular localization and organization of the MNPs. Because TEM microscopes operate under vacuum conditions, several processes were taken into account to prevent the membrane disruption and the dislocation of the organelles.

Cells were platted in two T75 cell culture flasks with 1 * 10^6 cells/mL each and incubated for 24h. 200 μg/mL of MNPs were then added in order to have a higher concentration of nanoparticles in the cells and incubated for 24h. After, the cells were washed three times with 5 mL of PBS and detached with 2 mL of trypsin-EDTA. Trypsin-EDTA was removed after centrifugation and the cells fixed with a solution of 3 % glutaraldehyde, at 0.12 M and pH 7.4, for 30 min, in a process that allows the preservation of live cell characteristics and therefore have accurate imaging [81].

To remove the glutaraldehyde, a 5 min centrifugation at 12000 rpm was performed, followed by three times washing step with a 0,12 M PBS, with 5 min centrifugation in-between at 7000 rpm.

The following step was to stain the sample with a 2 % osmium tetroxide, cover it with aluminum foil and stir for 3h. OsO_4 is used in TEM sample preparation to enhance contrast and allow better recognition of the cell membranes [82].

Due to the vacuum properties of the TEM, the cells should be depleted of their aqueous cytoplasm to further avoid organelle deformation. This step was done by washing the cells with solutions of increasing concentrations of acetone (two times each), starting at 30 % acetone in PBS until a final solution of 100 % acetone. Between each washing step a 10 min waiting was done, for the acetone to go inside the cell, drying the interior of cells.

TEM imaging samples must be laid in a copper grid and must be very thin. To be able to do such with a cell and preserve its integrity, the intracellular environment is replaced by a resin. The resin is composed of 21 mL of Durcupan™ ACM single component A, M epoxy resin (Sigma-Aldrich) and 180 µL of Durcupan™ ACM single component C, accelerator 960 (DY 060) (Sigma-Aldrich), and was used with decreasing concentrations of acetone with a waiting time of 1h between each use. The 100 % resin was added to the cells and left overnight. After it was removed and replaced by another 100 % resin. Finally, the sample was centrifugated, in order to create a pellet of cells, and incubated at 65 °C for 48h, to harden the resin.

Intracellular imaging requires that the cells are sliced in very thin cuts and placed in a copper grid. For the this step the pellet was sent and done in i3S - Instituto de Investigação e Inovação em Saúde, in Porto, Portugal.

TEM imaging was performed in a JEOL 2100 200 Kv TEM at INL facilities.

3.3.3. Sample preparation and Resazurin assay

Cell viability studies were performed on HeLa cell line, to assess the toxicity effect that the MNPs may have in for not being a biological product, a cell viability study was performed. Cells were plated in a 96 wells plate, with a cell density of $5 * 10^4$ cells/mL and incubated for 24h, to allow for cells to attach to glass surface and grow stress free.

A concentration dependent study, performed with a sequential dilution, was performed with a fixed time of 24h, represented in Figure 3.1. Resazurin at a concentration of 0.05 mg/mL was added, in a volume correspondent to 20 % the volume of cell culture medium present in the wells and incubated 1h before measuring.

Measurements were performed in a microtiter plate reader, equipped with Synergy H1MFD box and with the Gen5 controller software, with an electromagnetic excitation source of 560 nm.

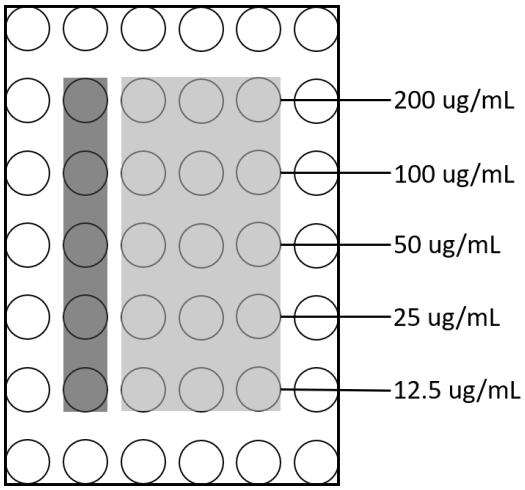

Figure 3.1 – Representation of the multi-well plate used to perform concentration dependent MNPs toxicity assay. Wells highlighted with dark and light grey were platted with a 5 * 10^4 cells/mL cell density. Light grey wells were incubated in with different Fe_3O_4 MNP concentration for 24h. 20 % of final volume of resazurin were added to dark and light grey wells. 100 µL of PBS were added to the white wells to avoid medium evaporation.

3.4. Sample preparation and nanothermometry studies

The main goal set was the implementation of a non-invasive fluorescence-based nanothermometry techniques to sense the intracellular temperature during hyperthermia treatment. Such experiments were done in a custom-built FLIM microscope.

3.4.1. Custom-built FLIM setup

The custom-built FLIM inverted microscope, represented in Figure 3.2, was composed of a vertically polarized picosecond laser, with a wavelength of 467 nm and tunable frequency, usually set at 20 MHz, PLP-10 from Hamamatsu.

To clean-up the laser profile, the beam is guided by two mirrors, M1 and M2 that allow for x an y axis beam movement, to a spatial filter composed of two lenses (f1=50 mm and f2= 50 mm, LA4148-A, Thorlabs), with f1 focusing in a 100 μm pinhole. A shutter is used to control the illumination and a clean-up filter (470.0 nm, 470FS10-25, Thorlabs) is used for securing the monochromaticity of the laser sources.

The laser is then reflected to a beam expander system composed of a pair of lenses (f1=40 mm and f2= 250 mm, AC254-040-B and AC254-250-B, Thorlabs) that is integrated into a cage system, and which is directly connected with the RM21 (MadCityLab), in which is mounted a 20x objective with 0.4 NA (M-20X, Newport), that is used to scan the sample. Scanning is performed by two piezo controlled positioners, micro and nanopositioner (NanoLPS200, MCL).

At the end of the 500 mm cage system can be found a kinematic 30 mm fluorescence filter cube (DFM1/M, Thorlabs), that is used to mount a 480LP Dichroic (F38-482, AHF Analysentechnik).

At the bottom of this kinematic cube a right-angle kinematic mount a mirror, M3, is used to guide the emission signal towards the output port, where a 25 μm spatial filter is mounted between a pair of lenses (f1 = 50 mm and f2 = 50 mm), after a 473 nm long-pass filter (AHF, F76-472).

The emission beam is then separated in the different polarizations by a polarizing beam splitter (Thorlabs), placed in a filter cube, that is then collected by two avalanche photodiode detectors (PD50CTD, MPD).

The Time Correlated Single Photon Counting (TCSPC) is implemented using a single-photon counting card (SPC130, Becker&Hickl) to which the sync of the pulsed laser source and the detector output (TTL pulses) are fed.

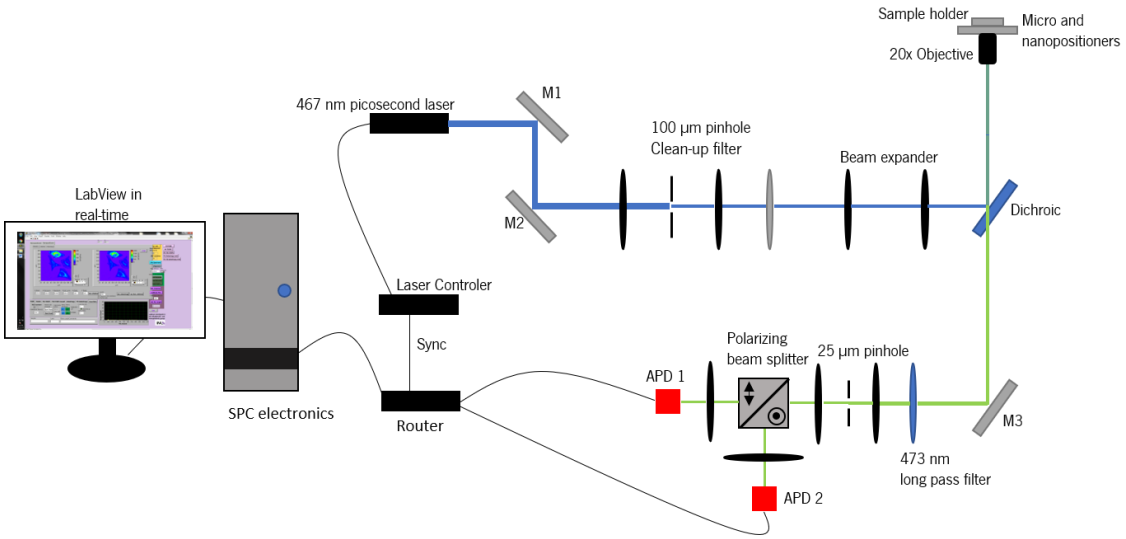

Figure 3.2 – Representation of the costum-built FLIM setup used for intracellular temperature measurements. A 467 nm picosend laser is guided by mirrors and a dichroic to a 0.4 NA 20x objective, that focused the laser beam in the sample and collected the fluorescence emission. This was then guided through a pinhole, to reduce emission from outside focal plane, into a polarizing beam splitter, that splits fluorescence emission in vertical and horizontal polarization, before reaching two APDs. The signal from the APDs is read by SPC electronics that enable TCSP. The is scanned with a micro and a nanopositioner, recording data in each pixel, allowing to build images in real-time by LabView based software.

An incubator with an electrically heated chamber and stage top incubator's controller (UNO-T-H-PREMIXED, H301-MCL-NANO-LPS, Okolab) is used for live cell imaging.

The controller software used is also custom-built, using the graphical language of LabView (National Instruments).

3.4.2. Sample preparation and FLIM/FPA measurements

FLIM and FPA measurements were performed in HeLa cells platted with a density of approximately 10^4 cells/mL inside two wells glued to the bottom of 35 mm diameter glass petri dish provided by Ibidi.

Intracellular fluorescence, emerald-GFP, was achieved by viral transfection, CellLight™ Actin-GFP, Mitochondria-GFP and BacMam GFP Transduction Control (BacMam 2.0, ThermoFisher). The transfection is performed through gene delivery by baculovirus, a modified insect cell virus.

Using the Actin-GFP and Mitochondria-GFP, transfection was done by adding 3 µL of viral solution after 24h incubation, while for the Transduction Control it was added immediately after platting.

MNPs were added to the sample 24h later, with a concentration of 50 μg/mL, and incubated overnight.

Temperature dependent measurements were performed by placing the petri dish in the microscope sample holder, equipped with water circulation system allowing precise temperature control. Temperature was monitored by means of placing an optical fiber immersed in the sample (nanoTherics) and images were acquired using FLIM setup described in chapter 3.4.1.

3.4.3. Alternating magnetic field exposure

For applying magnetic hyperthermia, the cells with MNPs were exposed to an alternating magnetic field. For such experiment an alternating magnetic field (AMF) generator device (nanoTherics), was provided by the Advanced (magnetic) Theranostic Nanostructures lab from the Nanomedicine group at INL – International Iberian Nanotechnology Laboratory.

The device used was composed of a frequency, voltage and current manual tuning for coil resonance (MagneTherm ™, nanoTherics), connected to an AMF enabled incubator for *in vitro* experiments that allows for live cell imaging, by creating an atmosphere of 5 % CO_2 (Live Cell Exposure Option, nanoTherics). Also, a circulating water (Recirculating Heater/Chiller, nanoTherics) enabled setting different environment temperatures that could be monitored by an immersed optical fiber attached to a temperature reader (Multi Channel Optical Sensing Signal Conditioner, nanoTherics).

The current frequency, voltage and intensity settings to generate a resonance with the coil, and therefore creating AMF of 20 mT strength, were 224.53 ± 20 KHz, 27.7 ± 1 V and 13.1 ± 1 A, respectively.

Magnetic hyperthermia treatment was applied, by firstly setting the water circulating temperature to 15 °C, to not damage the sample holder with the increasing temperature produced by the coil. The settings mentioned above were then manually set. With the alternating magnetic field on, a waiting time was established before starting data acquisition to avoid changes in the focal plane during imaging. The temperature was confirmed to be stable during same image acquisition window, after which the images were sequentially acquired, with focal plane adjustment.

Imaging was done in samples prepared as described in chapter 3.4.2 and acquired with setup described in chapter 3.4.1.

3.4.4. FLIM/FPA data analysis

The LabVIEW (National Instruments) based software developed for FLIM control, allows for real-time visualization of the data, but not for the analysis. For that the data is saved in hierarchical data format (hdf5) and binary (bin) files that can later be loaded in home developed MATLAB toolbox.

This program, allows for the visualization and analysis of fluorescence intensity, FLIM and FPA images with a user-friendly interface.

Fluorescence lifetime was calculated, using the total fluorescence intensity, that when collected by two detectors is given by Equation 3.1:

$$I_T = I_{II} + 2I_{\perp} \tag{3.1}$$

After, total fluorescence intensity image is then used to perform a multi-exponential fit, and therefore obtain the fluorescence lifetime value in each pixel. The data is then given in form of a FLIM image.

FPA calculations are done based on the same intensity images but applying Equation 2.14, where G factor value, 1.38, calculated with a sample of fluorescein in water, value can be set. In order to remove the background noise, the pixels outside the cell were set to for non-attributed number.

A smoothing function was also applied, that worked by averaging pixels with the nearest pixels.

The average, Equation 3.2, and standard deviation, Equation 3.3, values were obtained with the pre-inbuilt functions of MATLAB R2017a and used in OriginPro 2015 to create representative graphs.

$$\mu = \frac{1}{N}\sum_{i=1}^{N} A_i \tag{3.2}$$

$$S = \sqrt{\frac{1}{N-1}\sum_{i=1}^{N} |A_i - \mu|^2} \tag{3.3}$$

Where N is the number of observations and A is the measured value and N is the number of events.

Chapter IV – Results and discussion

4.1. Implementation and optimization of an FPA mode in the a FLIM setup

Fluorescence polarization anisotropy is a technique based on the polarization of the fluorescence emission. This property is closely related with the rotational movement of the fluorophore and can therefore be useful for the study of the microenvironment in which the emitting molecule is present. This detection of the different polarization components can be done in two different ways, either by detection of each component at different times, by rotation of a polarizer in the emission path, or detecting the two at same time by splitting the fluorescence emission in two components, with detection with different detectors. The latest is a more accurate approach, since it allows for the measurement of the same exact region at same time.

The custom-built microscope where intracellular temperature studies were performed initially was composed of one APD and had TCSPC capabilities, therefore was able to measure fluorescence lifetimes. Thus, for acquisition of both parallel and perpendicular polarizations at same time a second detector was implemented at 90° angle from the already existing one. Splitting the fluorescence emission in the polarization components was achieved by the placing a polarizing beam splitter.

Further system optimization was achieved by introducing a 25 μm pinhole before the beam splitter, providing better spatial resolution, since out focus collected fluorescence would be partially removed.

Real-time FPA imaging was also achieved by implementing Equation 2.14, in a customizable LabVIEW-based program. Such implementation can be seen in Figure 4.1, where “Hist. parallel” and “Hist. perp” are the fluorescence intensity of the parallel and perpendicular polarization component, respectively. Each pixel of the parallel and perpendicular intensity images is obtained by integration if the histogram of photon arrival per time bins. In the code G factor can be changed according to measurements conditions. AMF enabled incubator is compatible with micropositioner scanning stage. However, slow scanning speed of micro stage is incompatible with accurate temperature-dependent fluorescence measurements. Moreover, safety protocol of AMF equipment requires time operation to be less than 1 h. For faster imaging, an adapter to the nanopositioner

stage that has higher scanning speed was designed, Figure 4.2, and 3D printed with Witbox, BQ, at the Microfabrication and Exploratory Nanotechnology group, at INL.

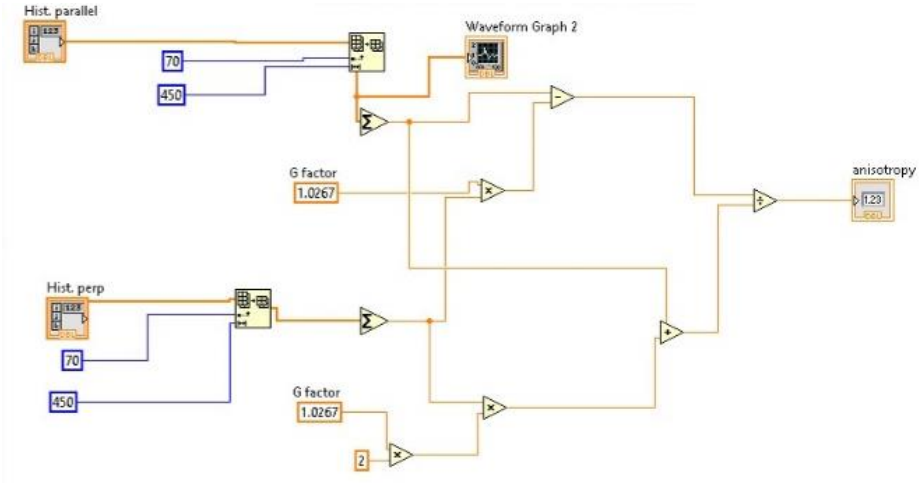

Figure 4.1 – Implementation of real-time FPA capabilities in the custom-built FLIM microscope. Fluorescence polarization anisotropy equation was implement in a program based in LabVIEW. Hist. parallel and Hist. perp, are the TCSPC decay curves of the parallel and perpendicular polarizations. Each curve is summed to obtain a fluorescence intensity value that is used to calculate FPA.

Figure 4.2 – Design of a 3D adapter to connect the AMF incubator to the piezo controlled nanopositioner during AMF. This was implemented using Sketchup software and printed with an Witbox, BQ device.

4.2. Characterization of the interaction of cells with MNPs

Before proceeding with temperature measurement experiments with magnetic hyperthermia treatment, uptake, intracellular localization and cell viability studies were performed.

4.2.1. Intracellular iron content determination

ICP-OES technique was used to calculate the amount of intracellular Fe present in the HeLa cells, and results are shown in Figure 4.3. The uptake studies were performed with two different concentrations of Fe_3O_4 nanoparticles and three different incubation times.

From Figure 4.3 it is evident that in both cases the nanoparticles are taken up by cells. At 50 µg/mL the lowest concentration inside the cells was seen at the 4h time point with 18.48 ± 0.11 pg/cell, while the highest was at 24 h with an uptake of 27.84 ± 0.11 pg/cell. For 100 µg/mL the lowest value was also at the 4 h time point with an average of 47.74 ± 0.20 pg/cell, while the highest was at 24 h, with 57.76 ± 0.24 pg/cell.

Thus, uptake difference for two concentrations is significant, 100 µg/mL concentration has almost two times higher uptake than 50 µg/mL.

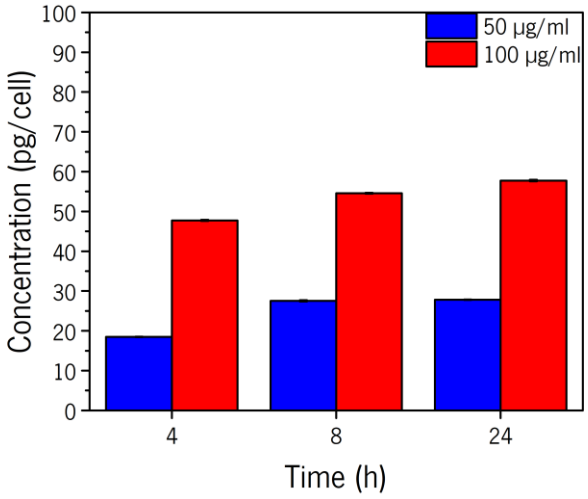

Figure 4.3 – Intracellular iron content of HeLa cells. Cells were incubated for different times, 4, 8 and 24 h with two different concentrations of Fe_3O_4 MNPs. Intracellular iron content was determined by ICP-ES. Incubation with 50 µg/mL is represented by blue bars, while red bars represent 100 µg/mL. Cells incubated with 100 µg/mL MNPs had approximately two times more iron than cells incubated with 50 µg/mL.

4.2.2. Intracellular localization of magnetic nanoparticles

Localization and distribution of the MNPs in HeLa cells were studied using imaging techniques. HeLa cells were incubated with 200 μg/mL nanoparticles during 24 h. Incubation with higher concentration of MNPs, than the ones used for uptake studies, was performed in order to assure high intracellular nanoparticles, thus allowing better recognition of their intracellular localization. Bright field transmission view of the cells, performed with confocal microscope, after incubation can be seen in Figure 4.4 A, where all of cells show dark agglomerates, mostly around the nucleus membrane. However, in order to identify the specific location of MNPs inside de cells, higher resolution images were obtained with TEM and shown in Figure 4.4. In the Figure 4.4 B image a nearly full HeLa cell can be seen with stained membranes due to sample preparation. Dark agglomerations around the nucleus membrane can be seen.

Magnified image of the agglomeration shown in Figure 4.4 C reveal presence of MNPs with approximate size of 10 nm.

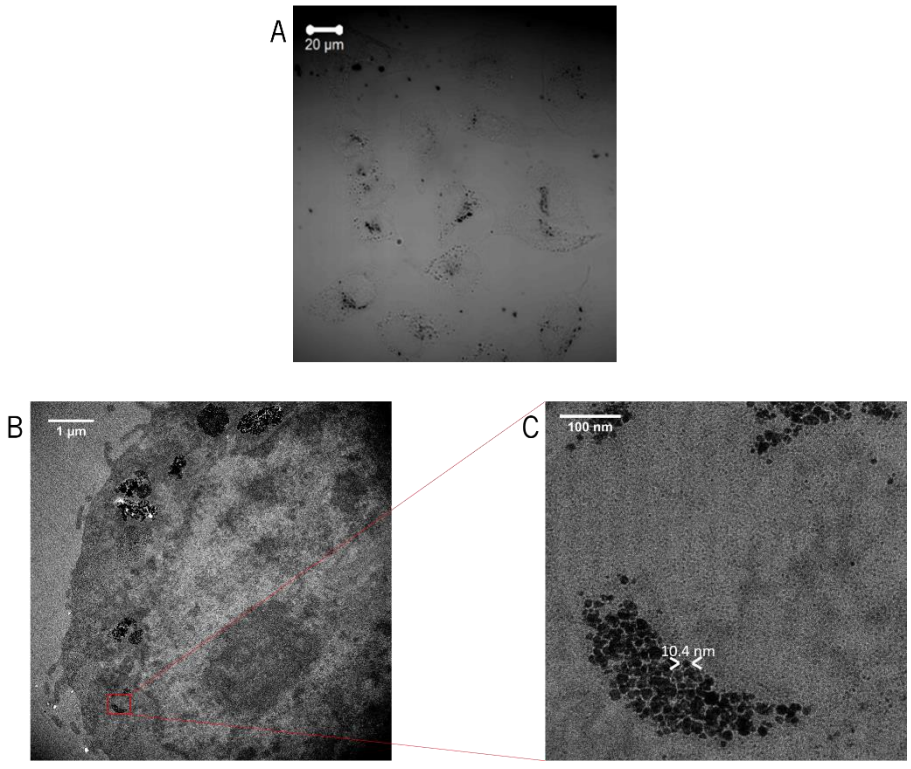

Figure 4.4 - Intracellular localization of Fe_3O_4 MNPs. Cells were incubated for 24 h with 200 μg/mL of MNPs, and localization determined by confocal and TEM imaging (move to the text). A) Confocal microscopy with 63x objective in transmission mode. B) Transmission electron microscopy. Both imaging techniques show nanoparticles agglomerated in the vicinities of the nucleus. Zoomed TEM image, demonstrates a single nanoparticles with 10.4 nm diameter.

4.2.3. Cell viability assay

The characterization of the interaction of the nanoparticles with cells was finalized with a resazurin cell viability assay, shown in Figure 4.5.

A concentration dependent study was performed in a 96 wells plate in which HeLa cells were platted and MNPs added in serial sequential dilution starting with 200 µg/mL, to cover a wide range of concentrations (0 – 200 µg/mL). After 24 h, resazurin was added in a volume 20 % of the cell culture medium.

In plot Figure 4.5, is evident that the cell viability increases from the control to the lowest concentration, 12.5 µg/mL. For higher concentrations, the cell viability decreases in a concentration dependent manner. Percentages lower than 80 %, are perceived as having low toxicity, which in the results obtained happens for concentrations equal or higher 100 µg/mL.

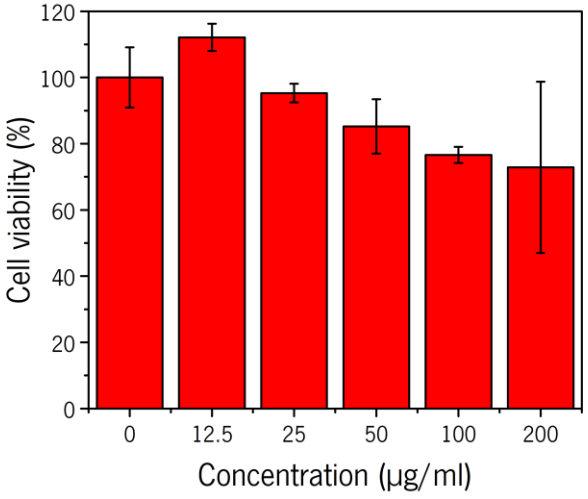

Figure 4.5 – Resazurin cell viability assay. HeLa cells were incubated for 24h incubation with different concentrations of Fe_3O_4 MNP, after which resazurin, 0.05 mg/mL, was added in volume equal to 20 % of the final volume and fluorescence intensity measured with an excitation at 560 nm. The percentagem of viable cells decreases with increasing concentration of nanoparticles. At 100 µg/mL the there is less than 80 %.

4.2.4. Discussion

Characterization of Fe_3O_4 MNPS interaction with HeLa cells, was assessed with three different experimental techniques to determine the intracellular iron content, the nanoparticle localization and the cell viability.

The uptake of these nanoparticles was determined by ICP-OES and plotted in Figure 4.3. This method allowed for the quantitative analysis of the intracellular iron content after incubation with different concentrations of MNPs. The results obtained showed a clear increase of intracellular iron in a concentration and incubation time dependent manner. The results obtained were similar to those found in literature, with increased intracellular iron content in cells incubated with higher MNPs concentration. *Wierzbinski et al. (2018)*, determined the uptake of Fe_3O_4 nanoparticles at a 48h time point, with a colorimetric experiment, using the Prussian blue staining assay, that has a dark pink color and when in contact with iron reduces ferric, Fe^{2+}, to ferrous, Fe^{3+}, that forms blue precipitates, to determine qualitatively the intracellular iron content, and by inductively couple plasma – mass spectroscopy, for quantitative measurements [83], [84]. *Liu et al. (2011)*, also determined the intracellular iron content of cells incubated with Fe_3O_4 nanoparticles coated with DMSA (Dimercaptosuccinic acid), by absorbance technique, reaching similar tendency, although with a lower one magnitude order [85].

Localization of such MNPs was determined in HeLa cells incubated with 200 μg/mL for 24 h, using a confocal and TEM microscope for imaging, where Figure 4.4, was obtained. Through both imaging techniques was possible to observe the distribution of nanoparticles in the vicinities of the cell nucleus. The same behavior was also observed with the use of the Prussian blue technique, where blue staining was seen around but not inside the nucleus, and also by TEM images, showing MNP aggregates round the nucleus [84], [85].

The final characterization study was cell toxicity with different concentrations of nanoparticles, ranging from 0 to 200 μg/mL. The results show a decrease in cell viability, through a decrease in their capacity to metabolize resazurin to resorufin. The study conducted by *Liu et al. (2011)*, included also a toxicity assay, with MTT, that is also based on metabolic ability, demonstrating similar results to the ones shown in Figure 4.5.

To sum up, the results achieved in the characterization of the interactions of Fe_3O_4 nanoparticles with HeLa cells are according to what was previously reported in literature. It is also important to highlight the fact that the concentration used for hyperthermia treatment, 50 μg/mL, conjugates

both a high uptake rate and an average cell viability above the 80 % that is, accordingly to the ISO 10993-5:2009, consider non-toxic and therefore appropriate to use *in vitro* studies [86].

4.3. Nontagged-GFP for intracellular temperature sensing during hyperthermia cancer treatments

In this subchapter temperature-dependent fluorescence lifetime and FPA measurements of HeLa cells transfected with BacMam GFP Transduction Control (BacMam 2.0, ThermoFisher), are presented (nontagged-GFP). This specific protein is expressed freely inside the cell and in all cell compartments.

In Figure 4.6 a confocal image, of nontagged-GFP transfected in a HeLa cell is shown. Excitation at 488 nm, induce fluorescence emission from emGFP arising from all over the cellular area.

4.3.1. Temperature dependent fluorescence studies of nontagged-GFP

Figure 4.7 A shows the fluorescence intensity images of HeLa cells platted and immediately transfected with nontagged-GFP. 50 µg/mL of MNPs were added and incubated overnight. Before imaging, cells were washed few times PBS followed by replacing culture medium. This procedure was fundamental to ensure that temperatures rising during magnetic hyperthermia would be due to MNPs taken up by the cell and not by the ones present in culture medium.

The sample was placed in the holder that enables the application of an alternating magnetic field, with a 5 % CO_2 atmosphere. Temperature-dependent imaging was acquired using the FLIM setup described in chapter 3.4.1. Temperature was set (15 – 37 °C) with a temperature-controlled water circulating system, and images of 100*100 micrometers were acquired with a resolution of one

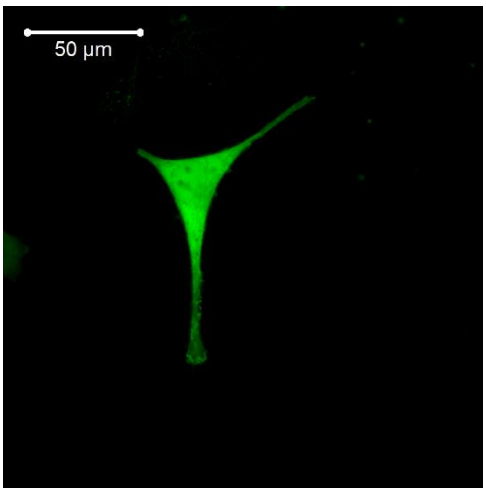

Figure 4.6 – HeLa cell transfect with nontagged-GFP. The tranfection leads to the GFP to be expressed in nontagged way in all cellular compartments.

pixel per micrometer, from the highest temperature, 37 °C in the water and 29 °C in the sample read by an optical fiber, to the lowest, 15 °C in the water and 18 in the sample. Such differences between the temperature of the circulating water and temperature measured by immersed optical fiber, are due to the laboratory environment, that has a room temperature of approximately 19 °C. Higher temperatures were not measured in order to preserve the cell viability and perform magnetic hyperthermia treatment in same healthy cell. The fluorescence intensity images were calculated from, Equation 3.1, described in chapter 3.4.4. As can be seen the shape and fluorescence intensity signal of the cell are similar to the one present in Figure 4.6, with fluorescence emission arising from all cellular structures. At the highest temperature tested, the fluorescence intensity was the highest, dropping in the second measurement and having similar intensity from there forward.

Fluorescence intensity images with parallel and perpendicular polarizations were recorded with two different APD, with setup explained in chapter 3.4.1, in order to calculate FPA images using Equation 2.14. The FPA images are present in Figure 4.7. The FPA image at 29 °C shows almost homogenous high FPA values all over the cellular area. As the temperature decreases, FPA increases until the 23.7 °C. At 20.9 and 18 °C a decrease of FPA is observed. Also, homogeneity of intracellular FPA is not observed with the center of the cell having higher FPA values than the rest of cellular structures.

The TCSPC acquired in each pixel during the measurements, allows to obtain a fluorescence lifetime value in each pixel. Figure 4.7 C shows the temperature-dependent fluorescence lifetime. As observed, fluorescence lifetime is not homogenous across the entire cell. The center of cells shows higher fluorescence lifetime values compared to more peripherical cell areas. Such central cell region seems to match with the higher fluorescence intensity in Figure 4.7 A. A pixel chosen from the regions with different fluorescence lifetime values, were used to plot the multi-exponential fitting along with the IRF used to calculate the fluorescence lifetime images. In the plots of Figure 4.7 D one can see that in the center region, the multi-exponential fitting at the two extreme temperatures although similar have different slopes. The same is observed in the periphery region, Figure 4.7 E, where multi-exponential decays at different temperatures present different slopes.

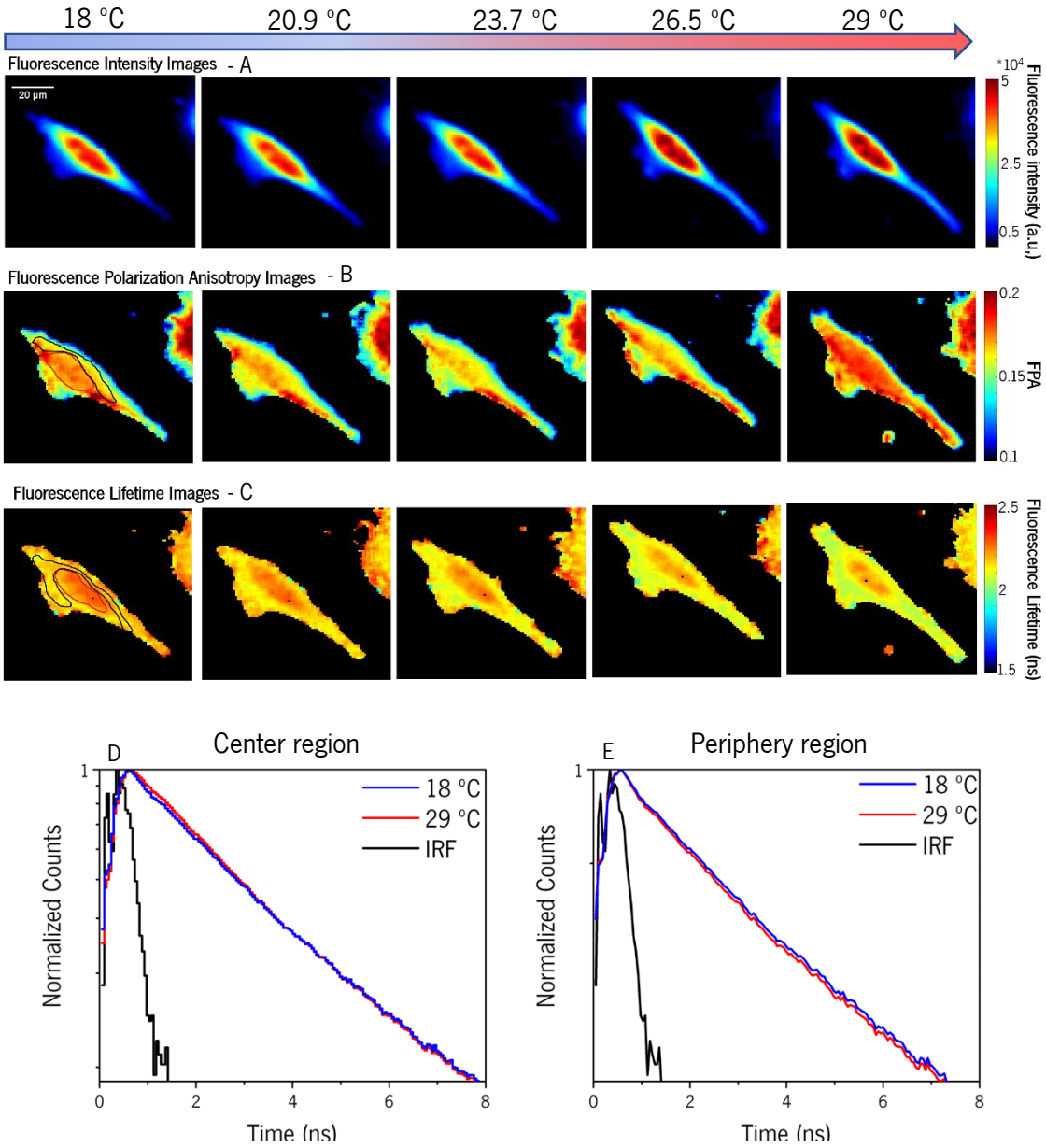

Figure 4.7 – Temperature dependent fluorescence studies. HeLa cell transfected with nontagged-GFP for 24 h after which 50 µg/mL were added and incubated overnight. Medium was removed and replaced by fresh one with risen step to remove not taken MNPs. Imaging was performed with a custom-built FLIM setup with controlled temperature set externally by circulating water bath and read by optic fiber immersed in sample medium. Fluorescence intensity images - A) Increase for higher temperatures. Fluorescence polarization anisotropy images – B) High heterogeneity in different regions of the cell and no clear dependency on temperature. Fluorescence lifetime images - C) Heterogeneity inside same cell, although visible decrease for higher temperatures. D) TCSPC multi-exponential fit of center region pixel shows no different between 18 and 29 °C. E) TCSPC multi-exponential fit of periphery region has different slopes at 18 and 29 °C.

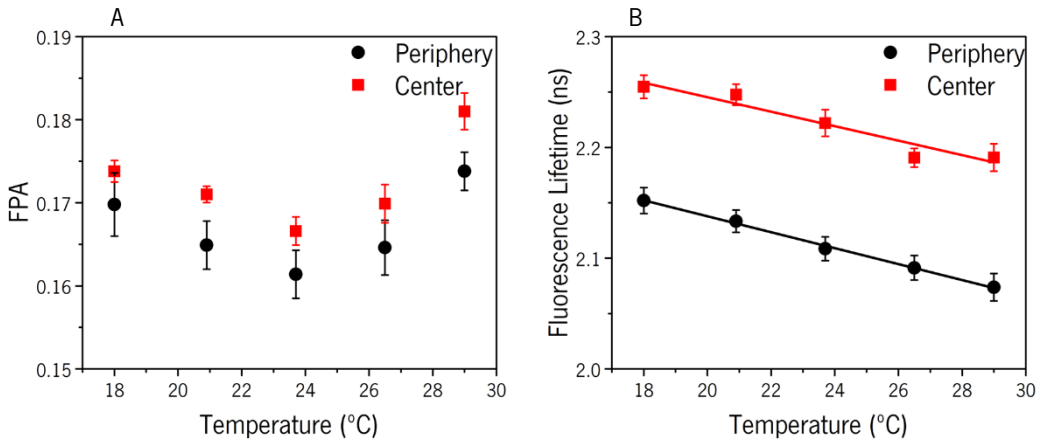

Figure 4.8 – FPA and fluorescence lifetime temperature dependency. Average and standard deviations of FPA and FLIM measured in single HeLa cell, labeled with nontagged-GFP and incubated with 50 µg/mL of Fe_3O_4 MNPs. Analysis was done in two separate regions and plotted with two different colors. Different regions were analyzed due to visible heterogeneity. A) FPA values do not follow a linear tendency. B) FLIM decreases linearly with increasing temperature.

Due to the inhomogeneous behavior of FPA and fluorescence lifetime, MATLAB R2017a software was used to separate two region of interest (ROI), with different components for higher and lower values. In Figure 4.8 A mean value FPA for the ROIs corresponding to center and periphery regions as function of temperature is shown. As temperature rising, FPA reduced degree of polarization due to the accelerated Brownian rotational motion of the fluorophore resulting in reduced degree of polarization. However, at 26 and 29 °C, FPA value increases. Figure 4.8 B shows temperature-dependent mean fluorescence lifetime for the same ROIs. It can be seen that fluorescence lifetime is decreasing linearly through entire temperature range, with approximately 10 ns different between the center and periphery regions

4.3.2. Magnetic hyperthermia treatment temperature sensing

After calibration measurements in chapter 4.3.1, the HeLa cells incubated with MNPs overnight were exposed to a 20 mT magnetic field, for magnetic hyperthermia treatment, generated with a 224.53 ± 20 KHz. The temperature set for the circulating water, was 15 °C in order to prevent damaging of the sample holder due to coil heating.

The images acquired at such treatment, are shown in Figure 4.9 with increasing AMF exposure times from left to the right. Equilibration time of an about 30 min was performed to ensure stable temperature inside the sample. The fluorescence intensity images at different time of AMF

exposure, are shown in Figure 4.9 A. It can be observed that fluorescence intensity is decreasing in all the cellular area with higher intensity in the center region, over whole-time range.

Same kind of behavior can be seen in FPA and fluorescence lifetime images presented in Figure 4.9 B and Figure 4.9 C. The fluorescence lifetime images show an overall decrease, with higher fluorescence lifetime in center region.

In order to follow the FPA and fluorescence lifetime behavior, same ROIs selected in the images of Figure 4.7 were used for image analysis of Figure 4.9. Mean value of FPA for the ROIs corresponding to center and periphery regions as a function of temperature are shown in Figure 4.10 A. It can be observed how FPA values linearly decrease with higher AMF exposure times in both center and periphery regions. The impossibility to fit the results shown in Figure 4.8, led to not calculate temperature with this fluorescence parameter.

Fluorescence lifetime measured in the two separate regions were plotted separately and shown in Figure 4.10, along with the temperatures deduced with the respective calibration curves. In these plots it is possible to observe a fluorescence lifetime decrease as AMF exposure times increase. Conversion to temperature allows to observe an increase in temperature. Temperatures achieved during magnetic hyperthermia treatment demonstrated to be higher in the center region, where temperatures above 70 °C were achieved, assuming fluorescence lifetime decreases linearly until such temperature.

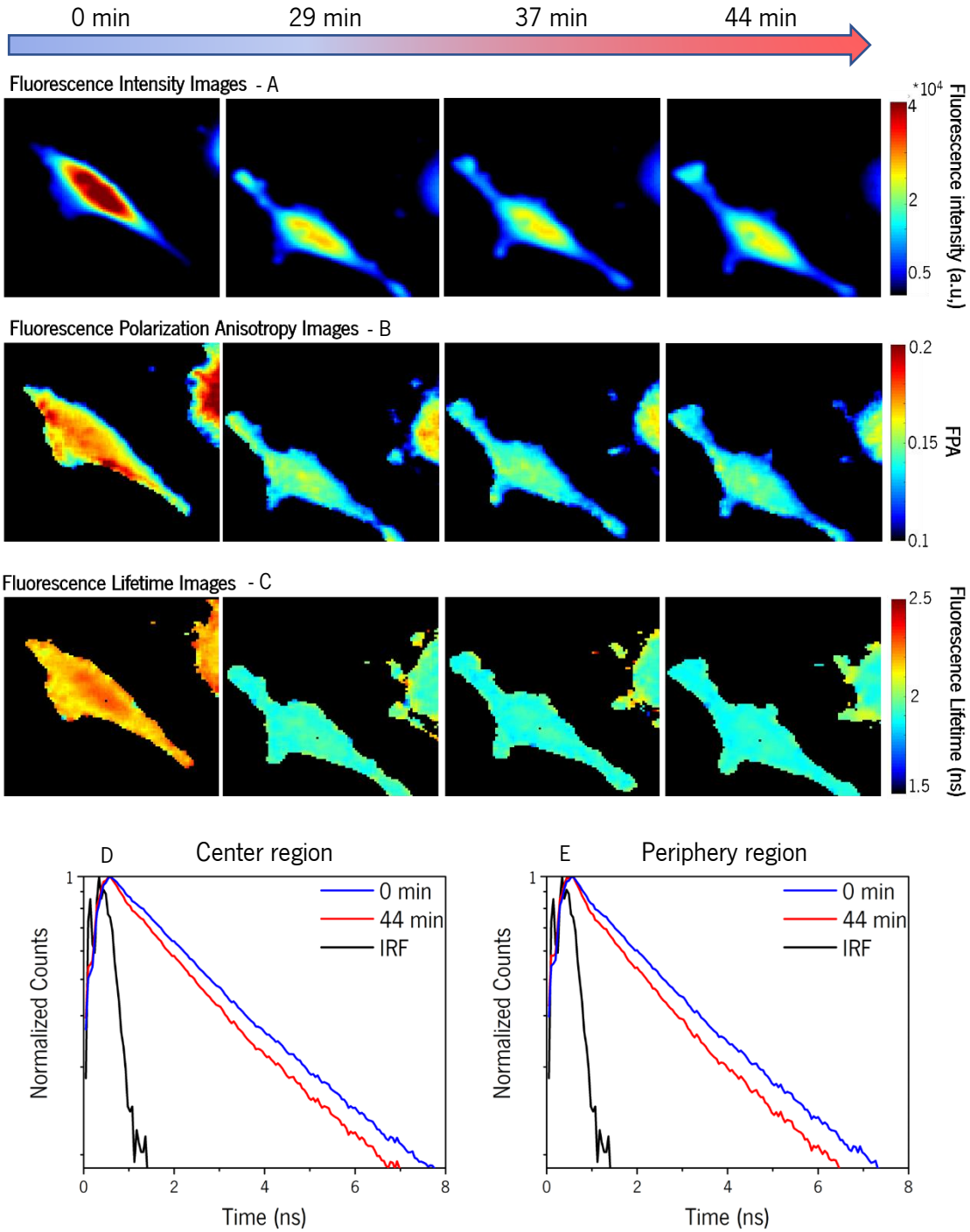

Figure 4.9 – Magnetic hyperthermia treatment dependent fluorescence studies. HeLa cell transfected with nontagged-GFP for 24 h after which 50 μg/mL were added and incubated overnight. Medium was removed and replaced by fresh one with risen step to remove not taken MNPs. Imaging was performed with a custom-built FLIM setup with applied 20 mT magnetic field, 224.53 ± 20 KHz and controlled external temperature set to 15 °C. Fluorescence intensity images – A) Decreased when exposed to AMF. Fluorescence polarization anisotropy images – B) Higher homogeneity with AMF exposure. Decrease is seen with higher exposure times. Fluorescence lifetime images – C) More homogenous when exposed to AMF. Values decrease for higher treatment times. D) TCSPC multi-exponential of center region fit shows different slope at 0 and 44 min. E) TCSPC multi-exponential fit in periphery region has different slopes at 0 and 44 min.

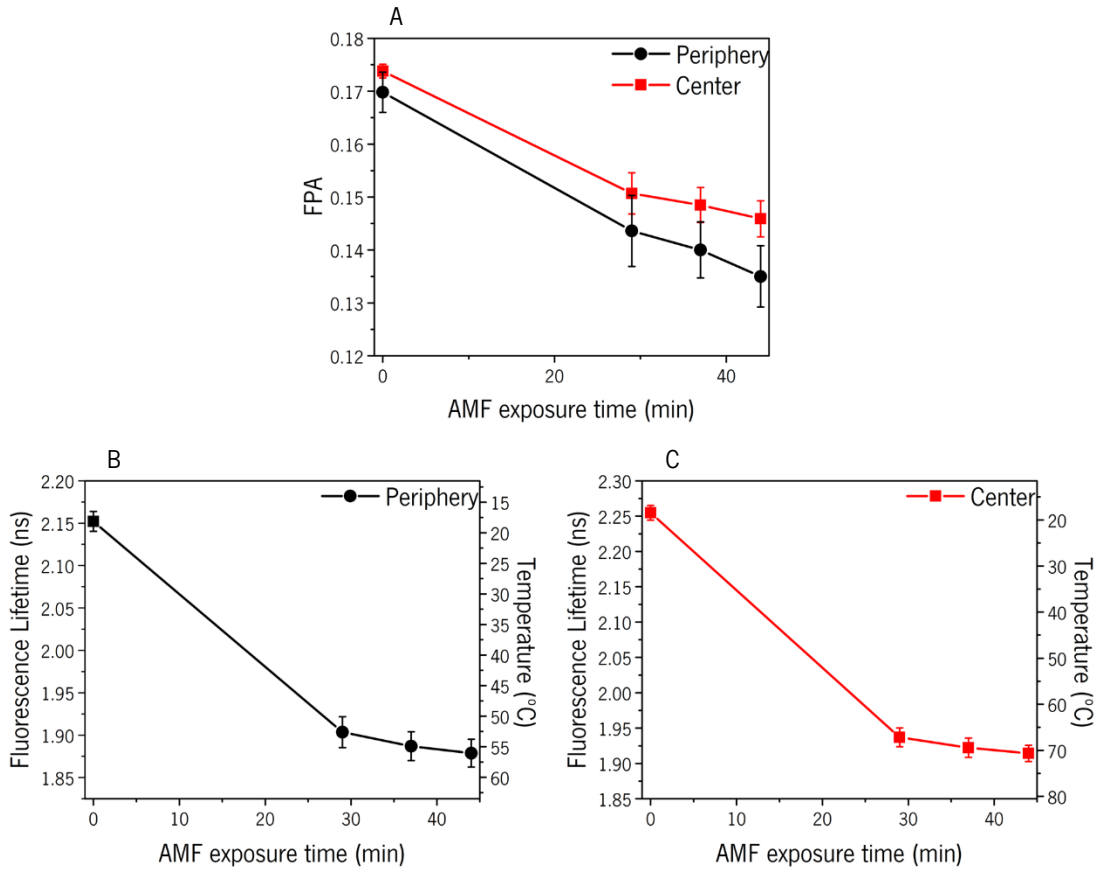

Figure 4.10 - FPA and fluorescence lifetime AMF exposure dependency. Average and standard deviations of FPA and FLIM measured in single HeLa cell, labeled with nontagged-GFP and incubated with 50 μg/mL of Fe_3O_4 MNPs while under 20 mT magnetic field. Analysis was done in two separate regions and plotted with two different colors. Same regions as in controlled temperature studies were analyzed. Intracellular temperature was deduced in the different regions with the respective equations. A) FPA values decrease linearly with higher exposure times. B) Fluorescence lifetime in center region decrease with higher exposure times. C) Fluorescence lifetime in periphery region decrease with higher exposure times. Highest deduced intracellular temperature of approximately 70 °C.

Equation obtained from the periphery and center regions plot of Figure 4.8 allowed for the temperature calculation in each pixel and therefore enabled to build a temperature map of the deduced intracellular temperatures. This images are shown in Figure 4.11 and can be seen, that although the plots of Figure 4.10, show a higher temperature in the center region, in the images the higher temperatures are achieved in the periphery of cell. Also, temperature increases from short to long AMF exposure. Interestingly is to notice that temperature seem to develop from the periphery to the center.

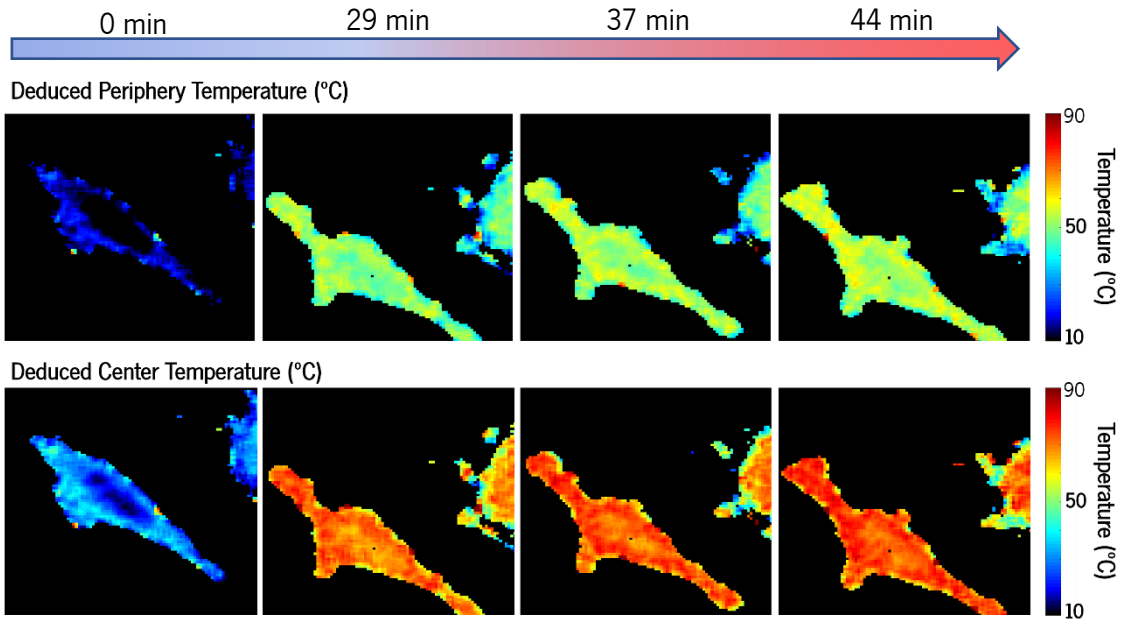

Figure 4.11 – Deduced intracellular temperature images. Temperature was calculated in pixel with the equations obtained from fluorescence lifetime linear fit. Temperature increase in entire cell body, with special focus in the periphery region.

4.3.3. Discussion

Confocal image of the nontagged-GFP HeLa cells shown in Figure 4.6 is in good agreement with fluorescence intensity image measured in FLIM setup (Figure 4.7 A). However, due to the absence of confocality in the FLIM setup, a major contribution of the GFP located in the center region of the cellular are can be observed.

Work performed by *Donner et al. (2012)*, demonstrated the use of nontagged-GFP to measure intracellular temperature in HeLa cells, by fluorescence polarization anisotropy, which decrease linearly in the range of temperature 20 - 40 °C [25]. The results showed in Figure 4.7 B, for the same type of measurement performed with temperature-controlled circulating water, demonstrated a linear decreased with rising temperature, but due to the focus drift in last temperature points we were not able to fully construct a calibration curve. From other side, AMF exposure induced heating of MNPs resulted in a substantial decrease of FPA presented in Figure 4.9 B. This contradiction in the results obtained from FPA measurements, leads to the assumption that while acquiring temperature dependent data, the time waited for the temperature to equilibrate through all the sample, 20 min, led to a change in focus, therefore to the imaging of a different focal plane, and

consequently different polarization. Moreover, time evolution of FPA during AMF exposure suggest continuous heating of MNPs.

During AMF exposure, the time frames between each of the images was much smaller, approximately 1 min to refocus, therefore reducing possibility of focus drift.

Also, the possible use of temperature-dependent fluorescence lifetime of nontagged-GFP was evaluated for intracellular temperature measurements. Up to our knowledge there are no studies on using fluorescence lifetime changes of GFP as temperature indicator. However, fluorescence lifetime-based luminescence intracellular temperature measurements can be found elsewhere [23], [87]. The results presented in Figure 4.7 C indicate linear decrease of fluorescence lifetime upon temperature rise. This dependence can be explained by the inversely proportional fluorescence lifetime with the rate of non-radiative energy loss, A_{nr} in Equation 2.11, that is increased at higher temperatures. Thus, fluorescence lifetime measurements are less affected by experimental conditions such as focus drift, excitation power fluctuation, concentration, etc. During magnetic hyperthermia treatment, a decrease of fluorescence lifetime values can be observed. This behavior can be attributed to the temperature rise of MNPs that located in the close vicinity to nontagged-GFP, upon AMF exposure.

However, fluorescence lifetime values are different in the center and periphery regions of the cellular area. Although having different values, the tendency with temperature rise is the same. This difference can be due to environmental temperature not being perceived in this region as in the rest of cell. During magnetic hyperthermia treatment, a temperature increase is induced by the magnetic actuation of the the MNPs inside the cell Temperature is sensed equally across the cell and therefore the values of fluorescence lifetime are more similar. Thus, the temperature values deduced from center region equation and plotted in Figure 4.10, where temperature is higher than in the periphery can be misleading.

The deduced temperature, Figure 4.11, determined by the equation deduced from linear fitting of both center and periphery regions of the cell demonstrate spots/areas with higher temperature Figure 4.11. It can be an indication of MNPs inside of HeLa cells, as demonstrated in TEM image of Figure 4.4.

In summary, FPA calibration measurements of nontagged-GFP expressed in HeLa cells did not enable for the use of this fluorescence parameter for intracellular temperature during magnetic hyperthermia treatment. However, during AMF exposure, reduced FPA values can be explained by higher molecular mobility as temperature increase and this parameter could be therefore used as

a nanothermometer. Also, for the first time, GFP temperature-dependent fluorescence lifetime was demonstrated to be a suitable of temperature. Fluorescence lifetime could be used to determine intracellular temperature, since the calibration curve showed a linear dependence of this fluorescence parameter with temperature changes. This property allowed for the successful intracellular temperature determination under magnetic hyperthermia treatment, assuming linear dependence until such temperature values.

4.4. Actin-GFP for intracellular temperature sensing during hyperthermia cancer treatments

In this subchapter temperature-dependent fluorescence lifetime and FPA done with HeLa cells transfected with CellLight™ Actin-GFP (BacMam 2.0, ThermoFisher), are presented. Actin is the most common intracellular protein and can be found in nearly all the cell volume. This protein can be found in two different forms, in monomers, as individual globular proteins, that are called G-actin or as filaments, in which the monomers polymerize to give structural support to cell [88], [89].

In Figure 4.12 a confocal image of actin-GFP HeLa cell is shown. Excitation at 488 nm, excites GFP molecules and therefore induces fluorescence emission that arise from actin filaments that cover all the cell area besides the nucleus, although more concentrated in the periphery regions. In the center regions, in nucleus vicinities, fluorescence emission from singular globular actin proteins is seen without defined shape.

4.4.1. Temperature dependent fluorescence studies of actin-GFP

Figure 4.13 A shows the fluorescence intensity image of a HeLa cell transfected with actin-GFP 24h after plating. 50 µg/mL of MNPs were then added and incubated with overnight. Before imaging performed with the custom-built FLIM setup, cells were washed several times with PBS

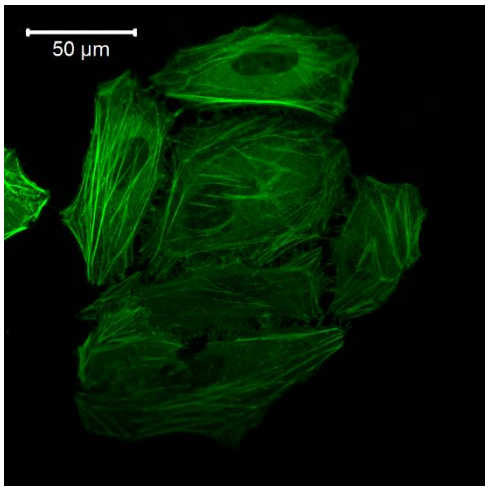

Figure 4.12 – HeLa cell transfect with actin-GFP. The transfection leads to the GFP to be expressed in a bound form to actin proteins. This protein can be found in a globular and free form r polimerized creatng filaments.

followed by culture medium replacement. This procedure was fundamental to assure that rising temperatures were caused by heat release from the MNPs taken up by the cell and not by the ones present in cell culture medium. The sample was placed in the incubator that allows AMF exposure with 5 % CO_2 atmosphere for optimal cellular growth conditions. Temperature-dependent images were acquired with a dimension of 100*100 micrometers, and one pixel per micrometer, from the highest to the lowest temperature, 37 to 15 °C, set for the water circulating system and 29.6 to 18.1 °C in the sample. Temperature reading was carried out by using an optical fiber immersed in the sample medium.

Fluorescence intensity images calculated from Equation 3.1, are shown in Figure 4.13 A. As can be observed shape is similar to those present in Figure 4.12, although fluorescence intensity is higher in the nucleus vicinities, decreasing gradually to the periphery. Also, can be seen that lower temperatures exhibit an overall higher fluorescence intensity than the ones measured at higher temperatures.

Temperature-dependent FPA images were determined from the recorded parallel and perpendicular polarization, using Equation 2.13, and can be seen in Figure 4.13 B. Images reveal inhomogeneous intracellular degree of polarization, with higher values in the surrounding nucleus region. FPA was the highest at a temperature of 20.6 °C, decreasing for higher temperatures. At 18.1 - 20.6 °C an increase is observed followed by a decrease up to 26.5 °C while at 26.5 – 29.5 °C there is an increase in FPA.

Fluorescence lifetime images, with multi-exponential fitting of TCSPC data acquired in each pixel, in dependence of temperature, are shown in Figure 4.13 C. Homogeneous intracellular actin-GFP fluorescence lifetime are observed. Different values are obtained from the nucleus region, that does not possess actin proteins. Also, fluorescence lifetime values decrease with increasing temperature in the entire measured temperatures range.

Figure 4.13 D pixel chosen from the highest fluorescence intensity region was used to plot the multi-exponential fitting of the TCSPC data along with the IRF used to calculate the fluorescence lifetime images. A clear difference in the slope at different temperatures is seen, resulting in different fluorescence lifetime.

Due to observed differences in the nucleus region, MATLAB R2017a was used to calculate mean and standard deviation of FPA and fluorescence lifetime, excluding the nucleus region. Figure 4.14 A shows such values of temperature-dependent FPA values, that decrease linearly in the

temperature range of 20.6 to 26.5 °C, although not following same decreasing behavior with increased temperature in the measured extreme temperatures.

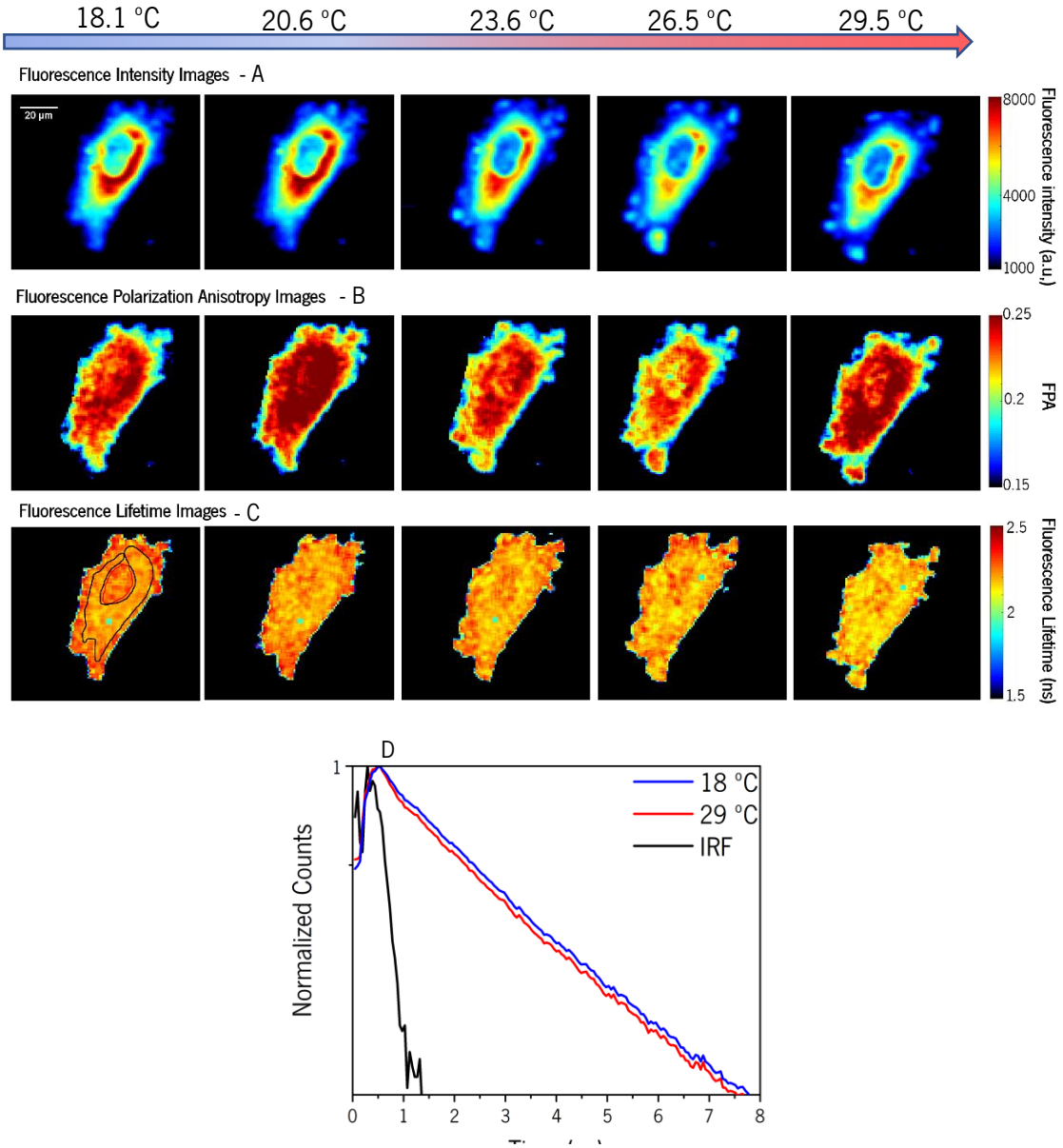

Figure 4.13 - Temperature dependent fluorescence studies. HeLa cell transfected with actin-GFP for 24 h after which 50 µg/mL were added and incubated overnight. Medium was removed and replaced by fresh one with risen step to remove not taken MNPs. Imaging was performed with a custom-built FLIM setup with controlled temperature set externally by circulating water bath and read by optic fiber immersed in sample medium. Fluorescence intensity images – A) Decrease with higher AMF exposure. Fluorescence polarization anisotropy images – B) Heterogeneity in different regions of the cell, no dependency on temperature is visible. Fluorescence lifetime images – C) Homogeneous values inside same cell, decrease can be seen for higher temperatures. D) TCSPC multi-exponential fit of has different slopes at 18 and 29 °C.

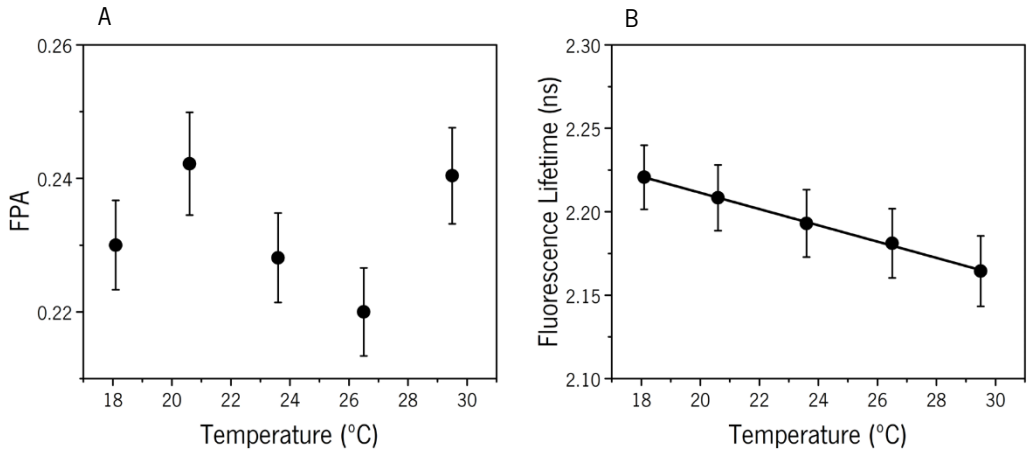

Figure 4.14 - FPA and fluorescence lifetime temperature dependency. Average and standard deviations of FPA and FLIM measured in single HeLa cell, labeled with actin-GFP and incubated with 50 μg/mL of Fe_3O_4 MNPs. A) FPA imaging does not follow a linear tendency. B) FLIM decreases linearly with increasing temperature.

In Figure 4.14 B, fluorescence lifetime in dependency of temperature are seen. A clear linear decrease is observed with higher temperatures.

4.4.2. Magnetic hyperthermia treatment temperature sensing

After temperature-dependent measurements, magnetic hyperthermia treatment was applied to same HeLa cell incubated overnight with 50 μg/mL MNPs, by exposing it at a 20 mT AMF. The temperature in water circulating was set to 15 °C, to avoid damages to the sample holder from heat generated by the coil. Images obtained under such conditions, are shown in Figure 4.15 with three different exposure times. In Figure 4.15 A one can observe that at first AMF exposure decreases the fluorescence intensity in the overall cellular area. Fluorescence intensity images recorded at higher exposure to magnetic hyperthermia treatment times show an increase in fluorescence intensity. Interestingly, in the nucleus vicinities a few spots remain with higher intensity, as well as in the periphery.

FPA images, obtained from parallel and perpendicular polarizations of actin-GFP transfected HeLa cells incubated with MNPs, while exposed to an AMF are shown in Figure 4.15 B. FPA values shown a decrease in the across entire cell throughout all the AMF exposure time range. Intracellular polarization heterogeneity observed in Figure 4.13 B remains, although higher FPA values are now observed in the periphery region.

Fluorescence lifetime images obtained from TCSPC multi-exponential fitting while under AMF exposure, are shown in Figure 4.15 C. While at magnetic hyperthermia treatment, fluorescence lifetime shows a decrease in entire range of time points. Also, fluorescence lifetime images in Figure 4.15 C are not as homogenous as the ones observed in the calibration experiments, Figure 4.13 C.

It is also worth noting that the spots of higher fluorescence intensity in Figure 4.15 A match with areas of both lower FPA and fluorescence lifetime, becoming more evident at higher exposure times.

TCSPC multi-exponential fitting, of a pixel selection from region similar to that of Figure 4.13 D shown in Figure 4.15 D, present a slope difference higher than seen in Figure 4.13 D, meaning larger fluorescence lifetime difference.

Mean values of FPA corresponding to all cellular area, excluding the nucleus are shown in Figure 4.16 A. A decrease in FPA is seen until 30 min of AMF exposure, after which there is an increasing. Fluorescence lifetime average values, shown in Figure 4.16 B, demonstrate a decrease of fluorescence lifetime throughout all the AMF exposure time range. Intracellular temperatures of HeLa cell incubated with MNPs and exposed to an AMF, for magnetic hyperthermia treatment were deduced from measured fluorescence lifetime values using linear fit of Figure 4.13 C. Average highest intracellular temperature was deduced to be approximately 80 °C.

Also, applying linear fit of Figure 4.13 C to fluorescence lifetime images of Figure 4.13 C, allowed reconstruction of deduced temperature images, shown in Figure 4.17. Intracellular temperatures increase with longer magnetic hyperthermia treatment times. High temperatures areas match high fluorescence intensity and low fluorescence lifetime spots seen in Figure 4.13 A and Figure 4.13 C, respectively. Also, shape and localization, nucleus vicinities, are similar to the ones seen in TEM image, Figure 4.4.

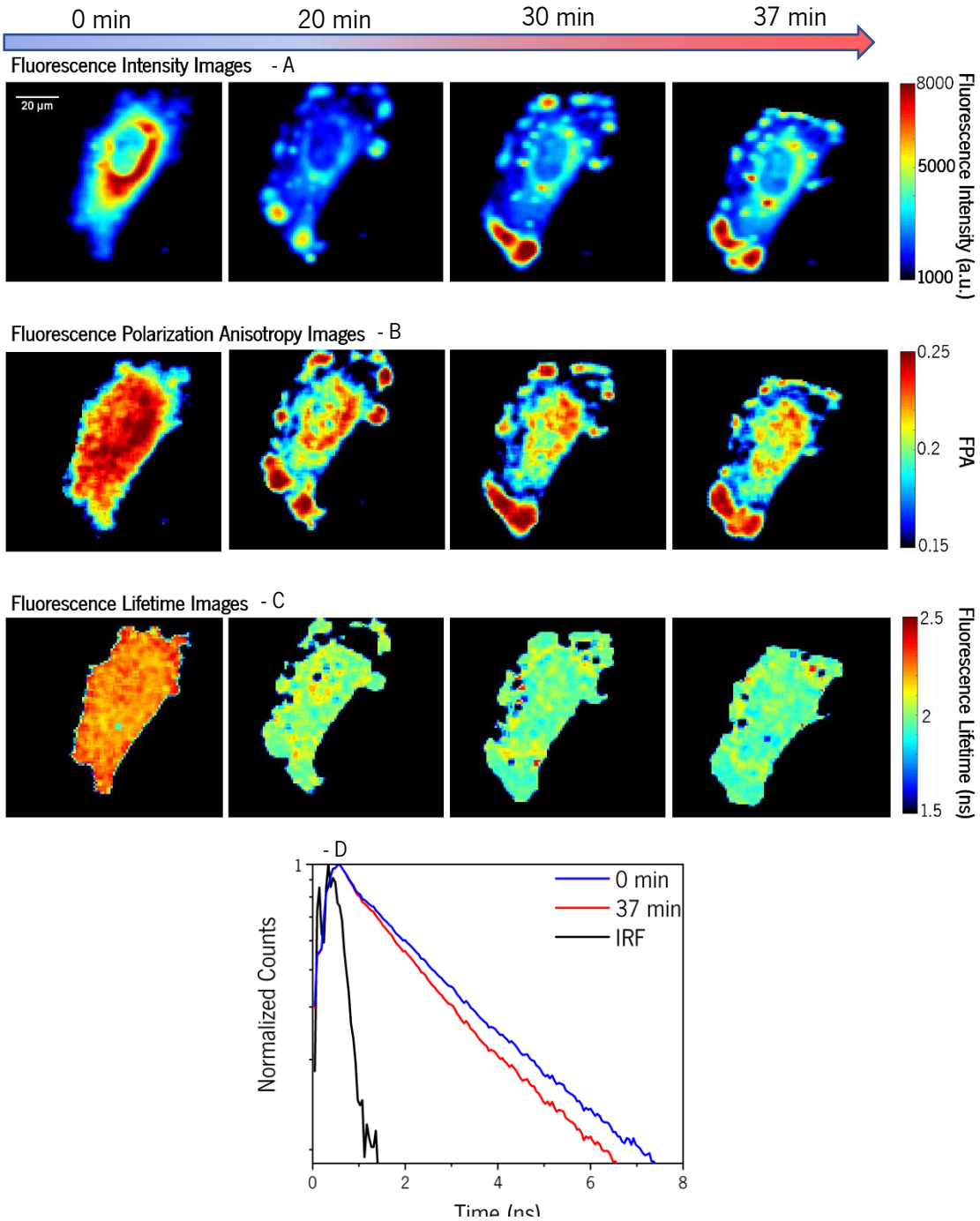

Figure 4.15 - Magnetic hyperthermia treatment dependent fluorescence studies. HeLa cell transfected with actin-GFP for 24 h after which 50 µg/mL were added and incubated overnight. Medium was removed and replaced by fresh one with risen step to remove not taken MNPs. Imaging was performed with a custom-built FLIM setup with applied 20 mT magnetic field, 224.53 ± 20 KHz and controlled external temperature set to 15 °C. Fluorescence intensity images – A) Decrease when compared to imaging performed before AMF exposure. Fluorescence polarization anisotropy images – B) Remains heterogeneous, decrease is seen with higher exposure times. Fluorescence lifetime images – C) More heterogeneus values, decreases with higher treatment times. E) TCSPC multi-exponential fit has different slopes at 0 and 37 min.

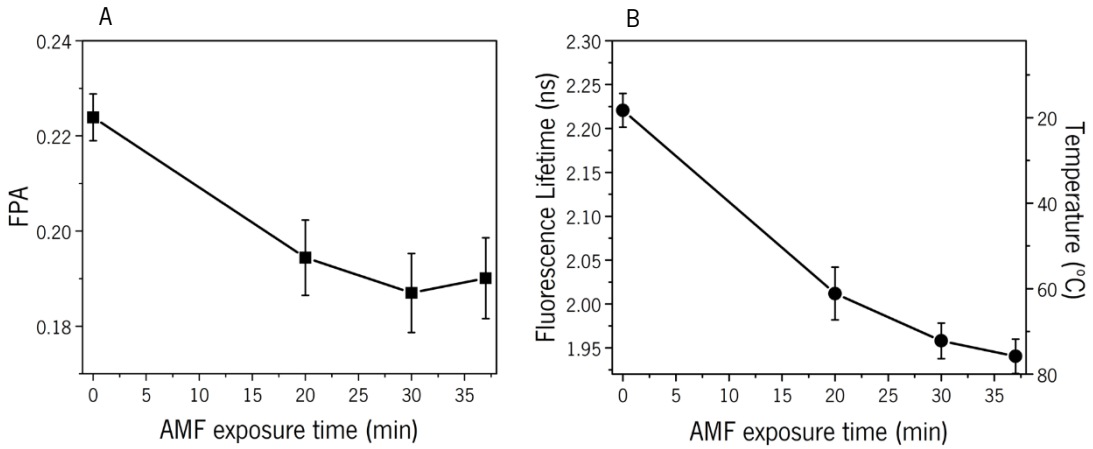

Figure 4.16 - FPA and fluorescence lifetime AMF exposure dependency. Average and standard deviations of FPA and FLIM measured in single HeLa cell, labeled with nontagged-GFP and incubated with 50 µg/mL of Fe_3O_4 MNPs while under 20 mT magnetic field. Intracellular temperature was deduced the respective equation. A) FPA values decrease linearly with higher exposure times. B) Fluorescence lifetime decrease at higher magnetic hyperthermia treatment exposure. Deduced intracellular temperature reached approximately 75 °C.

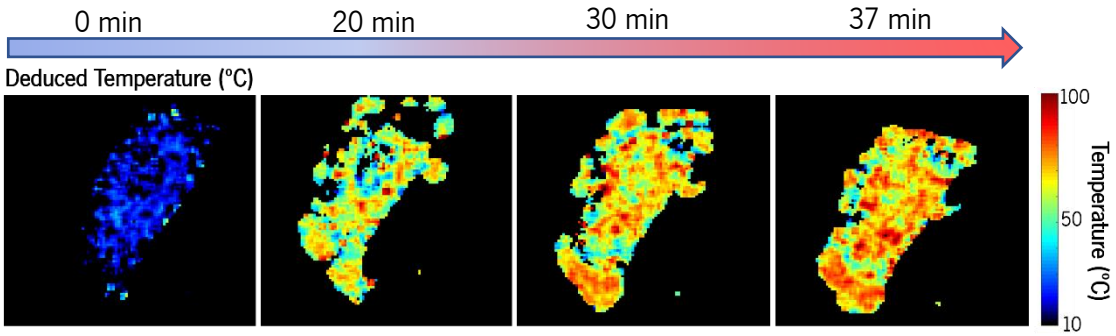

Figure 4.17 - Deduced intracellular temperature image. Temperature was calculated in pixel with the equation obtained from fluorescence lifetime linear fit. Temperature increase in entire cell body, with special focus in the periphery regions and some regions in the nucleus vicinities.

4.4.3. Discussion

HeLa cells were transfected with GFP attached to actin proteins. This type of protein can be found in the cell cytoplasm, in the monomer form or polymerized, forming filaments of consecutive actin proteins. Shape of fluorescence intensity images, shown in Figure 4.13 A recorded with FLIM setup, described in 3.4.1, are in agreement with the confocal image in Figure 4.12.

Vessoni Penna et al. (2004), demonstrated that GFP extracted from *Escherichia coli* would undergo up to 75 % denaturation for temperatures between 45 °C and 60 °C [90]. Fluorescence intensity images, in Figure 4.13 A, acquired with at known temperatures, showed small changes at different temperatures. During magnetic hyperthermia treatment the fluorescence intensity images shown in Figure 4.15 A was observed a decrease in fluorescence intensity values in overall cell area with special focus on the periphery regions. Such decrease is in good agreement to the ones report by *Vessoni Penna et al. (2004)* and can therefore be due to heat released from MNPs exposed to the AMF.

FPA measurements with cells transfected with actin-GFP were previously reported, with *Vishwasrao et al. (2012)*, coming to the conclusion that actin filaments report lower FPA values than the ones of globular actin. Authors explanation for such difference in FPA values, was based on the close proximity of the actin-GFP with different transition moment orientations [79]. Due to the overlap of absorption and emission spectrum of GFP a non-radiative transfer of energy, in a process known as Homo-Förster Resonance Energy Transfer (Homo-FRET) from a molecule in the excited stated (donor) to another in the ground state (acceptor), is possible. This phenomenon is reported to be the reason of lower degree of polarization in regions with predominance of actin filaments [53], [78], [91]. FPA images shown in Figure 4.13 B, allow the observation of the induced depolarization by Homo-FRET. Higher FPA values are seen in the nucleus vicinities, while in the periphery, where actin filaments are more predominant, FPA values are lower.

Temperature-dependent FPA imaging was performed, Figure 4.13 B, with mean FPA values demonstrated in Figure 4.14 A. A calibration curve was not fully constructed due to the deviation of the FPA values measured at 18.1 and 29.5 °C. The impossibility of a linear fit through the FPA data resulted in the impossibility to deduce intracellular temperature with this fluorescence parameter. During magnetic hyperthermia treatment, Figure 4.15 B, FPA values decreased until 30 min AMF exposure, after which a slight increase is observed. This behavior, observed with heat released in close proximity of the GFP molecules and the lower time between images, approximately 1 min to refocus, leads to assume that FPA could indeed be used to determine

temperature, and that the calibration experiment results were due to unfocusing effects led by the longer time waited for temperature equilibration, 20 min.

Although FPA values are altered by non-radiative interactions between molecules in close proximity, fluorescence lifetime is reported to be insensitive to such processes, as shown in homogenous fluorescence lifetime images of Figure 4.13 C [53], [78], [91].

Temperature-dependent FLIM studies, in Figure 4.13 C showed a linearly decrease with increasing temperature. Intracellular nanothermometry had never been reported with the use of actin-GFP as fluorescence lifetime nanothermometer.

Fluorescence lifetime images acquired during AMF exposure, Figure 4.15 C, showed a decreased in fluorescence lifetime throughout all the magnetic hyperthermia time range. The decrease in fluorescence lifetime can be explained with heat released of MNPs exposed to an AMF.

The successful determination of a temperature-dependent fluorescence lifetime allowed the calculation of intracellular temperature during magnetic hyperthermia treatment, the highest average intracellular temperature reaching approximately 80 °C. Localized heat production can be seen in Figure 4.17, in nucleus vicinities. This higher temperature spots are in agreement with observed shape and localization of MNPs in TEM image, Figure 4.4 B, and thus such high temperature can be explained by the close contact of the actin-GFP molecules and MNPs.

To summarize, the FPA measurements of actin-GFP transfected in HeLa cells did not follow the expected tendency in of FPA measurements during known temperature studies, not enabling the construction of a calibration curve and thus the impossibility to deduce intracellular temperature. During AMF exposure the values, decreasing FPA values demonstrated higher Brownian rotational motion of the fluorophore with increasing exposure time thus demonstrating that indeed it could be used for temperature determination.

A novel intracellular nanothermometer based on the fluorescence lifetime of actin-GFP was demonstrated and validated with the use in cells exposed to magnetic hyperthermia treatment.

4.5. Mitochondria-GPP for intracellular temperature sensing during hyperthermia cancer treatments

In this subchapter temperature-dependence FPA and fluorescence lifetime of HeLa cells transfected with CellLight™ Mitochondria-GFP (BacMam 2.0, ThermoFisher) are presented (mito-GFP). Mitochondria is a cellular organelle, that is result of the an endosymbiotic interaction between two different prokaryotic cells [92]. The main function of this organelle is now to produce energy for the cell in the form of ATP, making an important part of the cell metabolism, and therefore very interesting to study. The GFP used for the results shown in this chapter is attached to the E1 alpha pyruvate dehydrogenase, a domain of the pyruvate dehydrogenase protein which is located in the mitochondrial matrix, and has the function of converting pyruvate from glycolysis, to acetyl-CoA in the beginning of the tricarboxylic acid cycle [93].

Figure 4.18, shows a confocal image of HeLa transfect with mito-GFP. Upon excitation at 488 nm fluorescence emission can be observed from small regions in the vicinities of the nucleus.

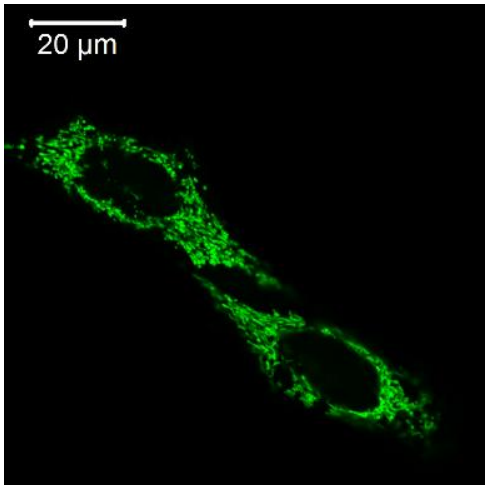

Figure 4.18 - HeLa cell transfect with mito-GFP. The tranfection leads to the GFP to be expressed in bound form to E1 alpha pyruvate dehydrogenase present in the mitochondrial matrix.

4.5.1. Temperature dependent fluorescence studies of mito-GFP

Sample of HeLa cell transfected with mito-GFP was placed in the holder that enables the application of an alternating magnetic field, with a 5 % CO_2 atmosphere. Temperature-dependent images were acquired using the FLIM setup described in chapter 3.4.1, and temperature set with a temperature-controlled water circulating system. Imaging was performed with dimension of 100*100 micrometers and a resolution of one pixel per micrometer, from the highest temperature, 37 °C in the water and 29.6 °C in the sample read by an optical fiber, to the lowest, 15 °C in the water and 18.3 in the sample.

Fluorescence intensity images, shown in Figure 4.19 A at 29.6 °C, is in agreement with confocal image of Figure 4.18, as fluorescence emission arises from a similar shaped small region around the nucleus. Decreasing temperature, change size of mitochondrial region, with a much smaller mitochondrial region seen in the imaged recorded at 26 °C, although with a defined nucleus.

FPA images obtained from the measurement of parallel and perpendicular polarization of fluorescence emission, are present in Figure 4.19 B. An increase of this fluorescence parameter with decreasing temperature is seen in the entire mitochondrial region and throughout all the measured temperature range.

Fluorescence lifetime images were determined from the TCSPC multi-exponential fitting in each pixel are shown in Figure 4.19 C. Fluorescence lifetime is observed to decrease for higher temperatures.

A representative multi-exponential fit was performed for the highest and lowest temperatures measured along with the IRF. It is clear from Figure 4.19 D, that the slope of fitted data acquired at 29.6 °C is steeper than the measured at 18.3 °C, therefore having lower fluorescence lifetime.

Mean and average values of FPA, were obtained with MATLAB R2017a, avoiding the nucleus region due to the absence of GFP in this organelle. Figure 4.20 A reveals linear decrease of mito-GFP polarization with increased temperatures.

Figure 4.20 B shows mean values of fluorescence lifetime in dependence of temperature. A linear decrease of fluorescence lifetime for higher temperatures is seen, although the measured 29.6 °C reveal further decreasing.

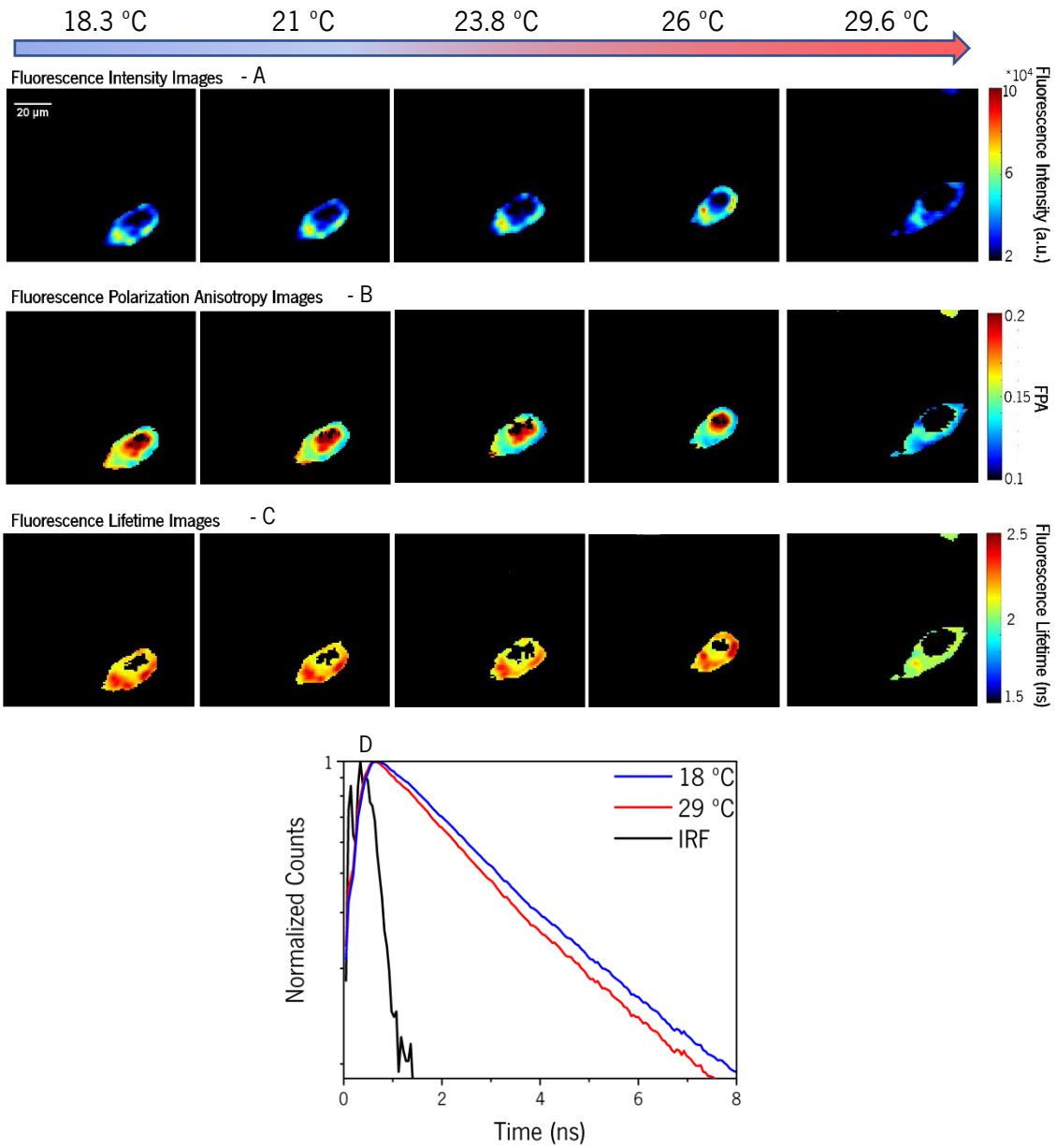

Figure 4.19 - Temperature dependent fluorescence studies. HeLa cell transfected with mito-GFP for 24 h after which 50 µg/mL were added and incubated overnight. Medium was removed and replaced by fresh one with risen step to remove not taken MNPs. Imaging was performed with a custom-built FLIM setup with controlled temperature set externally by circulating water bath and read by optic fiber immersed in sample medium. Fluorescence intensity images – A) No clear changes at different temperatures. Fluorescence polarization anisotropy images – B) Heterogeneity throughout entire cell with an increase FPA values at lower temperatures. Fluorescence lifetime images – C) Heterogeneity inside same cell, but a decrease is seen for higher temperatures. D) TCSPC multi-exponential fit has different slopes at 18 and 29 °C.

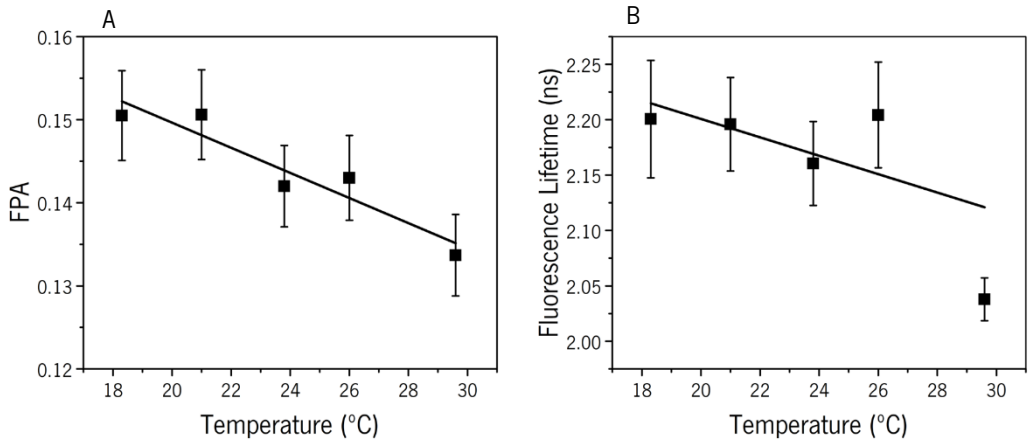

Figure 4.20 - FPA and fluorescence lifetime temperature dependency. Average and standard deviations of FPA and FLIM measured in single HeLa cell, labeled with mito-GFP and incubated with 50 μg/mL of Fe_3O_4 MNPs. A) FPA decrease linearly with increasing temperature. B) Fluorescence lifetime values decrease linearly with increasing temperature.

4.5.2. Magnetic hyperthermia treatment temperature sensing

Magnetic hyperthermia treatments were performed in a different mito-GFP transfected HeLa cell incubated with 50 μg/mL MNPs, due to the loss of cell viability of the one shown in Figure 4.19. Before imaging measurements, in order to ensure heat release from MNPs taken up by the cell rather than the ones present in culture medium, several washing steps with PBS were performed and culture medium replaced. Also, as the imaged cell was not the same as in calibration experiments, an image was acquired before AMF exposure, with a temperature of 15 °C in the circulating water and 18 °C in sample medium.

Fluorescence intensity images of HeLa cell exposed to magnetic hyperthermia treatment are shown in Figure 4.21 A. No changes of fluorescence intensity values can be observed when under AMF exposure.

FPA images, obtained with the measured parallel and perpendicular polarizations and calculated with Equation 2.13, are present in Figure 4.21 B. FPA values decrease in the entire mitochondrial region and in all measured exposure times.

Fluorescence lifetime images, with fluorescence lifetime values in each pixel, determined by multi-exponential fitting of collected TCSPC data, is observed in Figure 4.21 C. A decrease in

fluorescence lifetime values can be seen in all the fluorescence emission region and at all measured time points. Also, worth noticing that the values are homogeneous in the entire volume covered by this organelle.

In Figure 4.21 D a representative multi-exponential fitting, used in each pixel, can be seen for pixel selected in very close nucleus vicinity. No AMF and highest AMF time point exposure are represented along with IRF used.

Mean and average of FPA values, can be seen in Figure 4.22 A. A clear decrease of FPA values is seen in dependence of AMF exposure times. Also mean values of fluorescence lifetime can be seen in Figure 4.22 B. A steep decrease is seen for the 20 min exposure time, after which a linear decrease is observed.

As the cell exposed to magnetic hyperthermia treatment was different from the one imaged with controlled temperature, the obtained values of both FPA and fluorescence lifetime for the same temperature were different. Due to this difference the intracellular temperature could not be deduced, although it is worth noting that in the case of fluorescence lifetime the difference between before and during AMF exposure is higher than the one determined during controlled temperature.

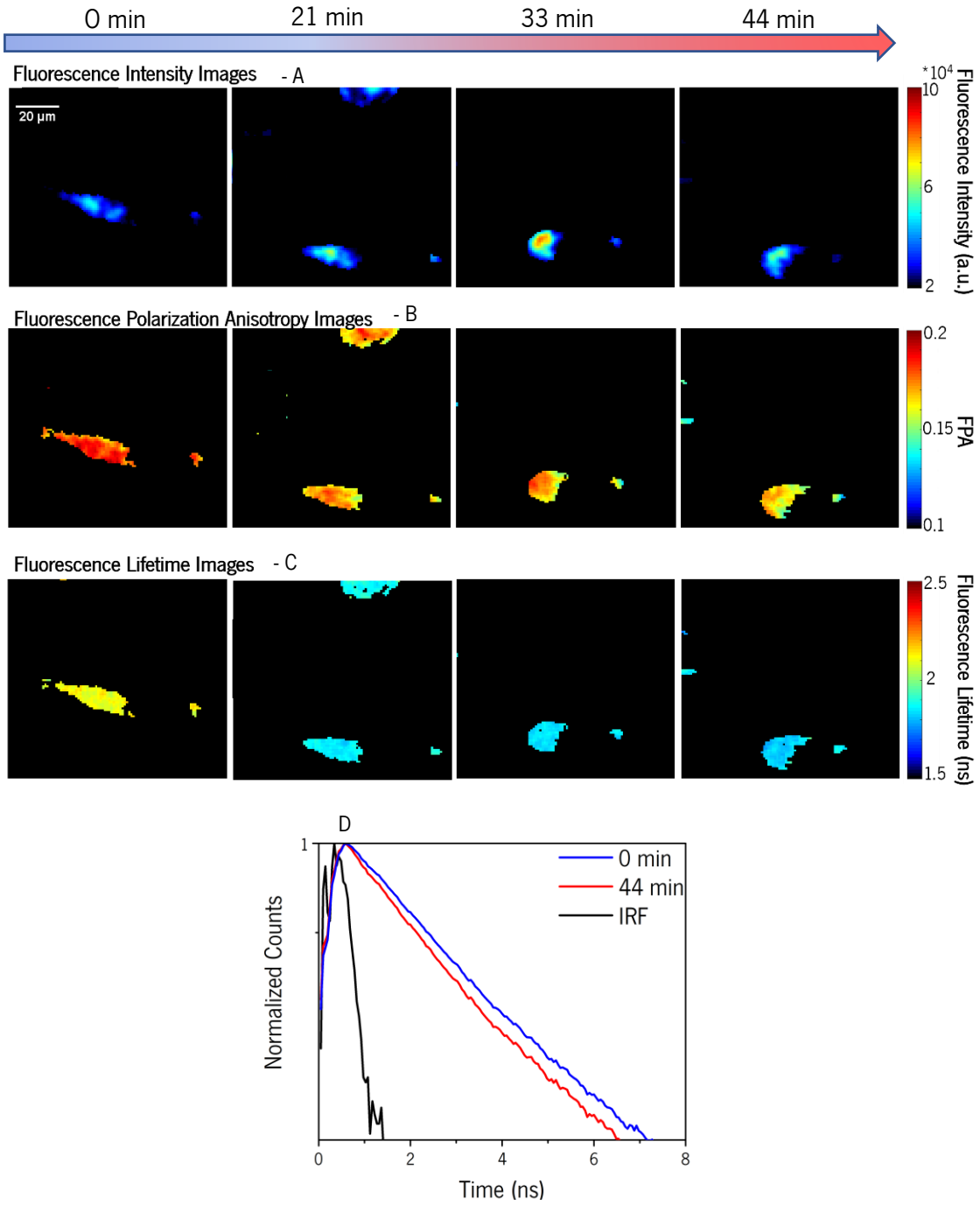

Figure 4.21 - Magnetic hyperthermia treatment dependent fluorescence studies. HeLa cell transfected with mito-GFP for 24 h after which 50 µg/mL were added and incubated overnight. Medium was removed and replaced by fresh one with risen step to remove not taken MNPs. Imaging was performed with a custom-built FLIM setup with applied 20 mT magnetic field, 224.53 ± 20 KHz with frequency of and controlled external temperature set to 15 °C. Fluorescence intensity images – A) No significative change at different temperatures. Fluorescence polarization anisotropy images – B) Homogeneity with decrease values at higher exposure times. Fluorescence lifetime images – C) More homogenous values decreasing at higher treatment times. D) TCSPC multi-exponential fit has different slopes at 0 and 44 min.

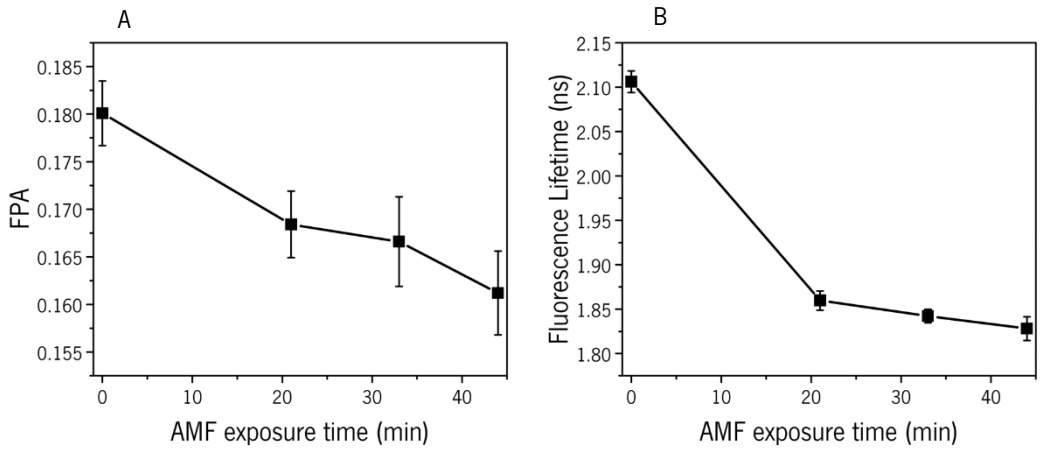

Figure 4.22 - FPA and fluorescence lifetime AMF exposure dependency. Average and standard deviations of FPA and FLIM measured in single HeLa cell, labeled with mito-GFP and incubated with 50 μg/mL of Fe_3O_4 MNPs while under 20 mT magnetic field. Intracellular temperature was deduced the respective equation. A) FPA values while under AMF exposure decrease linearly with higher exposure times. B) Fluorescence lifetime decreases with increasing AMF exposure time. Intracellular temperature was not deduced due to different values at same external temperature as in controlled temperature experiments.

4.5.3. Discussion

Temperature-dependent studies were performed with GFP transfected in the mitochondria, attached to the matrix protein pyruvate dehydrogenase, that is does the conversion of pyruvate from glycolysis to acetyl-CoA in the tricarboxylic acid cycle. The study of temperature is particularly interesting in this organelle, due to its metabolic functions that can lead to high temperatures. Recently has being reported, that temperatures as high as 50 °C were measured in the mitochondria, using the fluorescent probe MitoTracker Yellow [94].

Imaging with confocal microscope, demonstrated that indeed the fluorescence was only being emitted from small and very close to nucleus regions, and therefore from the mitochondria. Fluorescence intensity images, Figure 4.19 A, shows similar shape to those of Figure 4.18.

The measurements of both FPA and FLIM showed an increased heterogeneity, which lead to big deviations from the average value. The same behavior was also reported by *Kiyonaka et al. (2013)*, where the authors found that inside the same cell, different mitochondria could have different temperatures [95]. The reason for such differences can be explained from the differences in membrane potential, that is involved in the aerobic respiration process and therefore also directly involved in the production of energy in the form of ATP [96]. Observing the fluorescence lifetime

plots of Figure 4.22 B, one can see that the highest temperature measured is out of the linear fit. HeLa cells were firstly collected from a cervical cancer of a women, Henrietta Lacks, thus the optimal metabolic temperature is approximately 37 °C. As temperature in the circulating water was set to 37 °C, is possible to assume that the conditions for optimal metabolic activity were met, leading to higher temperature in this particular organelle, therefore lowering fluorescence lifetime values.

Even though a heterogeneity throughout all the mitochondria was observe, both FPA and fluorescence lifetime values demonstrated to decrease linearly with increased temperature.

At magnetic hyperthermia treatment with a different cell, is observable that the values of both measurements, before the AMF exposure, did not match with the ones from calibration experiments, once again proving the high heterogeneity found in this organelle.

Although this observation was made, upon applying alternating magnetic field was possible to see that the values of fluorescence lifetime had higher decrease than the ones in Figure 4.20 B. The difference between before and during magnetic hyperthermia treatment hugely surpass the difference between the lowest and highest temperatures measured during temperature-controlled imaging and can therefore be attributed to increased heat released by MNPs under AMF exposure.

4.6. Comparison of GFP based fluorescence labels as nanothermometers

The intracellular temperature was assessed by temperature dependence of two different fluorescence parameters by using three different GFP intracellular labels. Comparison of the relative sensitivity was made, calculated from the fitting curves of the controlled temperature experiments with Equation 1.1 and plotted in Figure 4.23.

Temperature-dependent FPA and fluorescence lifetime was assessed with nontagged-GFP in two separate regions, although only fluorescence lifetime values could be linearly fitted. Therefore, relative sensitivities were calculated for fluorescence lifetime in each region. Both calculated regions show higher sensitivity at higher temperatures. It is also possible to observe that the highest sensitivity in this type of fluorescent label was achieved in the periphery region, with a maximum relative thermal sensitivity of 0.35 %/°C.

Temperature dependent actin-GFP measurements were also fitted only for fluorescence lifetime, since no linear dependency was observed in FPA measurements. Relative sensitivity of this type GFP slightly increases with increasing temperature, ranging from 0.2 to 0.225 %/°C.

Mito-GFP was measured in only one region, as the fluorescence was emitted from same environment. This type of label was the only one showing a linearly temperature dependence in both fluorescence parameters, therefore it was the only one which the relative thermal sensitivity was calculated for FPA and FLIM. Interestingly is temperature-dependent FPA of mito-GFP, with a maximum relative sensitivity of 1.12 %/°C, has much higher relative thermal sensitivity than fluorescence lifetime, that has relative sensitivity similar to the other two labels.

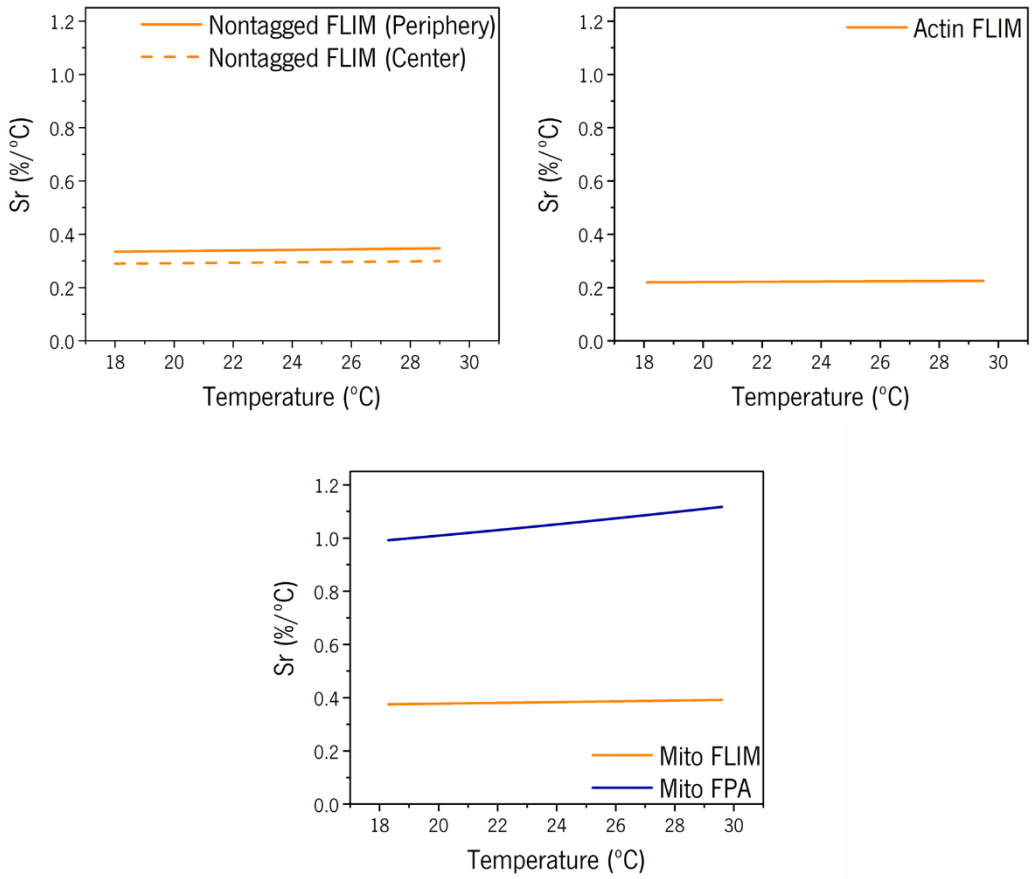

Figure 4.23 – Relative thermal sensitivities. Relative sensitivities were calculated from the fitted data of the measurements with controlled temperature. Two different sensitivities were calculated for nontagged-GFP due to heterogeneities, sensitivities increase upon temperature increase and the with highest sensitivity was achieved in the periphery region. Actin-GFP sensitivity also increases with temperature. Mito-GFP sensitivities were calculated for both FPA and FLIM, with the highest achieved in FLIM measurements.

4.6.1. Discussion

Relative thermal sensitivities were calculated with Equation 1.1, and shown in Figure 4.23, thus allowing comparison between the different targeting as well as the different temperature dependent fluorescent parameters used.

The relative thermal sensitivities determined from HeLa cells labeled with three differently targeted GFPs, were comparable when determined from the fitting curves of fluorescence lifetime measurements. Higher relative thermal sensitivity was achieved in the measurements of controlled temperature with mito-GFP labeled HeLa cells, using FPA as the temperature dependent fluorescence parameter.

The determination of such values allows also the comparison of the achieved sensitivities with other previously reported intracellular nanothermometers, that can be seen in Table 1. It is evident from this table that the sensitivity values achieved with fitted fluorescence lifetime values of GFP for fluorescence lifetime with GFP are similar to the estimated sensitivity achieved by *Donner et al. (2012)*, while the sensitivity determined from FPA measurements of GFP targeted to the mitochondrial matrix was found to be more sensitive to thermal variations than the one mentioned before [25], [97].

Comparing the nanothermometers developed during this work with other luminescent nanothermometers, one can observe that the sensitivity achieved from fittings of FPA values measured from mito-GFP are in the same order of magnitude.

The highest relative thermal sensitivities determined, were both measured fluorescence from the mito-GFP. Such values can be explained by the higher temperature of the mitochondria, that has higher metabolic activity at optimal temperatures, thus further decreasing values of the measured fluorescence parameters when external temperature approaches the optimal one, 37 °C.

Table 1 - Comparison of the relative thermal sensitivities of reported intracellular luminescent nanothermometers. (*) Estimated relative thermal sensitivity [97].

Material	$S_{r_{max}}$	Fluorescence Parameter	Thermal range	Localization	Cell type	Ref.
GFP	0.35 %/°C	Fluorescence Lifetime	18 – 29 °C	Cytoplasm	HeLa	[This work]
GFP	0.23 %/°C	Fluorescence Lifetime	18 – 29 °C	Actin proteins	HeLa	[This work]
GFP	0.4 %/°C	Fluorescence Lifetime	18 – 29 °C	Mitochondria	HeLa	[This work]
GFP	1.1 %/°C	FPA	18 – 29 °C	Mitochondria	HeLa	[This work]
GFP	0.4 %/°C *	FPA	20 - 40 °C	Cytoplasm	HeLa, U-87 MG	[25]
ER thermo yellow	3.9 %/°C	Fluorescence Intensity	32 - 37 °C	Endoplasmic reticulum	HeLa	[98]

Mito thermo yellow	2 - 2.8 %/°C	Fluorescence Intensity ratio	37 – 42 °C	Mitochondria	HeLa, NIH3T3, C2C12, mESC, Chang, BAT	[99]
Mito-RTP	2.72 %/°C	Fluorescence Intensity ratio	25 – 43 °C	Mitochondria	HeLa	[100]
Ru(bpy) 32+doped silica NPs	1.26 %/°C	Fluorescence Intensity	25 – 45 °C	Cytoplasm	HepG2	[101]

The fluorescent probes used in this work as nanothermometers were tested during the exposure, of HeLa cells incubated with 50 μg/mL, to magnetic hyperthermia treatment

Heat produced by similar Fe_3O_4 nanoparticles was assessed by *Dong & Zink (2014)*, in which they found that in solution the temperature rapidly increased when a 375 kHz alternating magnetic field was applied and could sense a temperature change of 20 °C after 1.5 min after which a temperature continued to increase at a slower rate, reaching approximately 30 °C after 5 min [102].

The temperatures calculated with nanothermometry implement and demonstrated in this work, show a big gradient of temperature According to the TEM images in Figure 4.4, magnetic nanoparticles accumulated in the nucleus vicinities, where temperature rise above 50 °C regions. Temperature calculated with fluorescence lifetime-based actin-GFP demonstrated the highest temperatures, with regions reaching temperatures more than 80 °C, maybe due to the fact that the heat effectors (MNPs) in this specific case are in close contact with GFP. Deduced temperatures images calculated from fitting equations of temperature-dependent FPA and fluorescence lifetime at the mitochondria were not built due to the fact that measurements at same external temperature were observed to have different values. Although such images were not shown, one can observe that the heat release from the MNPs was also sensed by fluorescence lifetime measurements, as the difference between before and during AMF exposure, 0.28 ns, was higher than at the ones seen between lowest and highest temperatures measured with controlled temperature, 0.17 ns.

Such high temperatures achieved could be due to the use of a magnetic field, 20 mT, that is four times stronger than the ones used in clinical trials. Also, one can see that the time of exposure in this work was much higher than those of *Dong &Zink (2014)*, maximum 5 min AMF exposure [102].

Chapter V – Conclusions and future perspectives

The work shown in this thesis had as objective and goals the implementation and validation of established and novel fluorescence based intracellular nanothermometry.

To achieve such goals the optimization of a FLIM setup from one detector to a two-detector setup was done along with a polarizing beam splitter, allowing for simultaneous detection of fluorescence emission with different polarizations, thus enabling the easier use of fluorescence polarization anisotropy. Also, a 25 μm pinhole was successfully implemented in the emission path which improved the microscope resolution. Further improvement was done with the 3D printing of an adapter for the AMF enabled incubator, allowing fast imaging.

In vitro studies were performed with HeLa cells, which were thawed and maintained as a cell culture. The interaction of MNPs with this cell line was studied by three different ways. It was successfully proven by ICP-ES that MNPs were taken up by the cells in a concentration and time dependent manner. Intracellular localization of MNPs was assessed by both confocal microscopy and TEM, with images demonstrating similar localization in the nucleus vicinities. Also, toxicity studies were performed with the resazurin assay, that showed concentration dependent toxicity and enabled to select a safe MNPs concentration for further experiments.

Fluorescence based nanothermometry, was possible due to transfection of HeLa cells with three different types of GFP fluorophores. The conventional FPA could not be used for intracellular nanothermometry, since a temperature dependence was not observed during the temperature-controlled experiments. Although FPA did not result as expected, intracellular temperature was assessed with fluorescence lifetime, which had never been reported for this type of fluorescent label and can therefore be considered as a novel intracellular nanothermometer.

Finally, the nanothermometry techniques used to determine the intracellular temperature were validated *in vitro* during magnetic hyperthermia treatment, with results showed that intracellular temperatures significantly increase during this treatment. The highest average temperature measured, was approximately 80 °C, in spots with similar localization to that of the MNPs showed by TEM.

In the future and in order to more accurately sense the intracellular temperature with higher sensitivity, a further optimization of the FLIM setup should be made. Also, studies with different MNPs concentration, different magnetic fields and shorter time points could be performed to

optimize the experimental magnetic hyperthermia conditions, in such a way that the maximum temperature achieved is approximately 42 °C.

Chapter VI - References

[1] S. H. Hassanpour and M. Dehghani, "Review of cancer from perspective of molecular," *J. Cancer Res. Pract.*, vol. 4, no. 4, pp. 127–129, 2017.

[2] L. N. Kwong and L. Chin, "The Metastasis Problem Gets Stickier," *Cancer Cell*, vol. 15, no. 1, pp. 1–2, 2009.

[3] P. S. Steeg, "Targeting metastasis," *Nat. Rev. Cancer*, vol. 16, no. 4, pp. 201–218, 2016.

[4] "Cancer Tomorrow." [Online]. Available: http://gco.iarc.fr/tomorrow/graphic-isotype?type=1&population=900&mode=population&sex=0&cancer=39&age_group=value&apc_male=0&apc_female=0. [Accessed: 09-Oct-2018].

[5] B. Hildebrandt, "The cellular and molecular basis of hyperthermia," *Crit. Rev. Oncol. Hematol.*, vol. 43, no. 1, pp. 33–56, 2002.

[6] J. van der Zee, "Heating the patient: A promising approach?," *Ann. Oncol.*, vol. 13, no. 8, pp. 1173–1184, 2002.

[7] L. Shi, O. Kwon, A. C. Miner, and A. Majumdar, "Design and batch fabrication of probes for sub-100 nm scanning thermal microscopy," *J. Microelectromechanical Syst.*, vol. 10, no. 3, pp. 370–378, 2001.

[8] S. Sadat, A. Tan, Y. J. Chua, and P. Reddy, "Nanoscale thermometry using point contact thermocouples," *Nano Lett.*, vol. 10, no. 7, pp. 2613–2617, 2010.

[9] A. Balčytis, M. Ryu, S. Juodkazis, and J. Morikawa, "Micro-thermocouple on nano-membrane: Thermometer for nanoscale measurements," *Sci. Rep.*, vol. 8, no. 1, pp. 8–13, 2018.

[10] Y. Yue and X. Wang, "Nanoscale thermal probing," *Nano Rev.*, vol. 3, no. 1, p. 11586, 2012.

[11] C. D. S. Brites *et al.*, "Thermometry at the nanoscale," *Nanoscale*, vol. 4, no. 16, pp. 4799–4829, 2012.

[12] G. Tessier, M. Bardoux, C. Boué, C. Filloy, and D. Fournier, "Back side thermal imaging of integrated circuits at high spatial resolution," *Appl. Phys. Lett.*, vol. 90, no. 17, p. 171112, 2007.

[13] T. Favaloro, J. Bahk, and A. Shakouri, "Characterization of the temperature dependence of the thermoreflectance coefficient for conductive thin films Characterization of the temperature dependence of the thermoreflectance coefficient for conductive thin films,"

Rev. Sci. Instrum., vol. 86, p. 024903, 2015.

[14] Z. Amira, M. Bouyahi, and T. Ezzedine, "Measurement of Temperature through Raman Scattering," *Procedia Comput. Sci.*, vol. 73, pp. 350–357, 2015.

[15] T. Qin *et al.*, "Organic fluorescent thermometers: Highlights from 2013 to 2017," *TrAC - Trends Anal. Chem.*, vol. 102, pp. 259–271, 2018.

[16] K. Okabe, R. Sakaguchi, B. Shi, and S. Kiyonaka, "Intracellular thermometry with fluorescent sensors for thermal biology," *Pflugers Arch. Eur. J. Physiol.*, vol. 470, no. 5, pp. 717–731, 2018.

[17] S. Uchiyama, C. Gota, T. Tsuji, and N. Inada, "Intracellular temperature measurements with fluorescent polymeric thermometers," *Chem. Commun.*, vol. 53, no. 80, pp. 10976–10992, 2017.

[18] S. Uchiyama and C. Gota, "Luminescent molecular thermometers for the ratiometric sensing of intracellular temperature," *Rev. Anal. Chem.*, vol. 36, no. 1, 2017.

[19] M. Nakano and T. Nagai, "Thermometers for monitoring cellular temperature," *J. Photochem. Photobiol. C Photochem. Rev.*, vol. 30, pp. 2–9, 2017.

[20] S. Uchiyama *et al.*, "A Cell-Targeted Non-Cytotoxic Fluorescent Nanogel Thermometer Created with an Imidazolium-Containing Cationic Radical Initiator," *Angew. Chemie - Int. Ed.*, vol. 57, no. 19, pp. 5413–5417, 2018.

[21] Y. Takei *et al.*, "A nanoparticle-based ratiometric and self-calibrated fluorescent thermometer for single living cells," *ACS Nano*, vol. 8, no. 1, pp. 198–206, 2014.

[22] G. Kucsko *et al.*, "Nanometre-scale thermometry in a living cell," *Nature*, vol. 500, no. 7460, pp. 54–58, 2013.

[23] K. Okabe, N. Inada, C. Gota, Y. Harada, T. Funatsu, and S. Uchiyama, "Intracellular temperature mapping with a fluorescent polymeric thermometer and fluorescence lifetime imaging microscopy," *Nat. Commun.*, vol. 3, pp. 705–709, 2012.

[24] R. Tanimoto *et al.*, "Detection of Temperature Difference in Neuronal Cells," *Sci. Rep.*, vol. 6, no. September 2015, pp. 1–10, 2016.

[25] J. S. Donner, S. A. Thompson, M. P. Kreuzer, G. Baffou, and R. Quidant, "Mapping intracellular temperature using green fluorescent protein," *Nano Lett.*, vol. 12, no. 4, pp. 2107–2111, 2012.

[26] J. S. Donner *et al.*, "Imaging of plasmonic heating in a living organism," *ACS Nano*, vol. 7, no. 10, pp. 8666–8672, 2013.

[27] M. Hurwitz and P. Stauffer, “Hyperthermia, radiation and chemotherapy: The role of heat in multidisciplinary cancer care,” *Semin. Oncol.*, vol. 41, no. 6, pp. 714–729, 2014.

[28] P. Wust *et al.*, “Hyperthermia in combined treatment of cancer,” *Lancet Oncol.*, vol. 3, no. 8, pp. 487–497, 2002.

[29] S. Jha, P. K. Sharma, and R. Malviya, “Hyperthermia: Role and Risk Factor for Cancer Treatment,” *Achiev. Life Sci.*, vol. 10, no. 2, pp. 161–167, 2016.

[30] M. Bañobre-López, A. Teijeiro, and J. Rivas, “Magnetic nanoparticle-based hyperthermia for cancer treatment,” *Reports Pract. Oncol. Radiother.*, vol. 18, no. 6, pp. 397–400, 2013.

[31] A. H. Morrish, “Diamagnetic and Paramagnetic Susceptibilities,” *Phys. Princ. Magn.*, pp. 31–77, 2001.

[32] A. H. Morrish, “Ferromagnetism,” *Phys. Princ. Magn.*, vol. 1664, no. 1960, pp. 259–331, 2001.

[33] N. A. Frey, S. Peng, K. Cheng, and S. Sun, “Magnetic nanoparticles: Synthesis, functionalization, and applications in bioimaging and magnetic energy storage,” *Chem. Soc. Rev.*, vol. 38, no. 9, pp. 2532–2542, 2009.

[34] C. T. Yavuz *et al.*, “Low-Field Magnetic Separation of,” *Science (80-.).*, vol. 314, no. 5801, pp. 964–967, 2006.

[35] Q. Li, C. W. Kartikowati, S. Horie, T. Ogi, T. Iwaki, and K. Okuyama, “Correlation between particle size/domain structure and magnetic properties of highly crystalline Fe3O4nanoparticles,” *Sci. Rep.*, vol. 7, no. 1, pp. 1–4, 2017.

[36] Q. A. Pankhurst, J. Connolly, J. S. K, and J. Dobson, “Applications of magnetic nanoparticles in biomedicine,” *J. Phys. D. Appl. Phys.*, vol. 36, pp. R167–R181, 2003.

[37] Wahajuddin and S. Arora, “Superparamagnetic iron oxide nanoparticles: Magnetic nanoplatforms as drug carriers,” *Int. J. Nanomedicine*, vol. 7, pp. 3445–3471, 2012.

[38] M. Hofmann-Amtenbrink, B. von Rechenberg, and H. Hofmann, “Superparamagnetic nanoparticles for biomedical applications,” in *Advanced drug delivery reviews*, vol. 65, no. 5, 2009, pp. 119–149.

[39] F. Shubitidze, K. Kekalo, R. Stigliano, and I. Baker, “Magnetic nanoparticles with high specific absorption rate of electromagnetic energy at low field strength for hyperthermia therapy,” *J. Appl. Phys.*, vol. 117, no. 9, 2015.

[40] K. Kekalo, I. Baker, R. Meyers, and J. Shyong, “Magnetic Nanoparticles with High Specific Absorption Rate at Low Alternating Magnetic Field,” *Nano Life*, vol. 5, no. 2, 2016.

[41] M. Johannsen, B. Thiesen, P. Wust, and A. Jordan, “Magnetic nanoparticle hyperthermia for prostate cancer,” *Int. J. Hyperth.*, vol. 26, no. 8, pp. 790–795, 2010.

[42] T. Matsubara, K. Kusuzaki, A. Matsumine, and K. Asanuma, “A Minimally Invasive Surgery for Bone Metastases Using the Combination of Photodynamic Therapy and Hyperthermia Treatment,” *Int. J. Clin. Med.*, vol. 4, no. August, pp. 357–363, 2013.

[43] A. Jabłoński, “Efficiency of Anti-Stokes Fluorescence in Dyes,” *Nature*, vol. 131, no. 3319, pp. 839–840, 1933.

[44] R. J. D. Tilley, “Light and Colour,” in *Colour and the Optical Properties of Materials: An Exploration of the Relationship Between Light, the Optical Properties of Materials and Colour*, 2nd ed., John Wiley & Sons, Ed. 2011, pp. 1–47.

[45] E. A. Permyakov, “Energy Levels in Molecules and Transition Between Them,” in *Luminescent Spectroscopy of Proteins*, 1st ed., Boca Raton: CRC Press, 1993, pp. 5–34.

[46] G. G. Stokes, “On the Change of Refrangibility of Light,” *Philos. Trans. R. Soc. London*, no. 142, pp. 463–562, 1852.

[47] J. R. Lakowicz, “Introduction to Fluorescence,” in *Fluorescence Polarisation/Anisotropy in Diagnostics and Imaging*, 3rd ed., Springer US, 2006, pp. 1–25.

[48] “The Nobel Prize in Chemistry 2008 - Press release.” [Online]. Available: https://www.nobelprize.org/prizes/chemistry/2008/press-release/. [Accessed: 27-Aug-2018].

[49] Y. Shibata *et al.*, “Cloning full-length, cap-trapper-selected cDNAs by using the single-strand linker ligation method,” *Biotechniques*, vol. 30, no. 6, pp. 1250–1254, 2001.

[50] S. Schmidt *et al.*, “Silica Nanoparticles for Intracellular Protein Delivery: a Novel Synthesis Approach Using Green Fluorescent Protein,” *Nanoscale Res. Lett.*, vol. 12, 2017.

[51] M. Kneen, J. Farinas, Y. Li, and a S. Verkman, “Green fluorescent protein as a noninvasive intracellular pH indicator.,” *Biophys. J.*, vol. 74, no. 3, pp. 1591–1599, 1998.

[52] A. D. Kummer, C. Kompa, H. Niwa, T. Hirano, S. Kojima, and M. E. Michel-Beyerle, “Viscosity-dependent fluorescence decay of the GFP chromophore in solution due to fast internal conversion,” *J. Phys. Chem. B*, vol. 106, no. 30, pp. 7554–7559, 2002.

[53] K. Suhling *et al.*, “Fluorescence lifetime imaging (FLIM): Basic concepts and some recent developments,” *Chem. Phys. Lett.*, vol. 27, pp. 3–40, 2015.

[54] J. R. Albani, “Fluorescence Spectroscopy Principles,” in *Principles and Applications of Fluorescence Spectroscopy*, Blackwell Publishing, 2008, pp. 88–114.

[55] F. Dörr, “Spectroscopy with Polarized Light,” *Angew. Chemie Int. Ed. English*, vol. 5, no. 5, pp. 478–495, 1966.

[56] A. Jabłoński, “A Note on the Notion of Emission Anisotropy,” *Bull. L’Académie Pol. des Sci. Série des Sci. math., astr. phys.*, vol. X, no. 10, pp. 555–556, 1962.

[57] H. Zhang, Q. Wu, and M. Y. Berezin, “Fluorescence anisotropy (polarization): from drug screening to precision medicine,” *Expert Opin. Drug Discov.*, vol. 10, no. 11, pp. 1145–1161, 2015.

[58] G. Baffou, M. P. Kreuzer, F. Kulzer, and R. Quidant, “Temperature mapping near plasmonic nanostructures using fluorescence polarization anisotropy,” *Opt. Express*, vol. 17, no. 5, p. 3291, 2009.

[59] F. Perrin, “Polarisation de la lumière de fluorescence. Vie moyenne des molécules dans l’etat excité,” *J. Phys. Radium,* vol. 7, no. 12, pp. 390–401.

[60] C. B. Boss and K. J. Fredeen, “General Characteristics of ICP-OES,” in *Concepts, Instrumentation and Techniques in Inductively Coupled Plasma Optical Emission Spectrometry*, 3rd ed., Shelton: PerkinElmer, pp. 2-1-2–12.

[61] “Press release: The 1986 Nobel Prize in Physics.” [Online]. Available: https://www.nobelprize.org/prizes/physics/1986/press-release/. [Accessed: 23-Aug-2018].

[62] W. T. Gunning and E. P. Calomeni, “A Brief Review of Transmission Electron Microscopy and Applications in Pathology,” *J. Histotechnol.*, vol. 23, no. 3, pp. 237–246, 2000.

[63] M. Winey, J. B. Meehl, E. T. O’Toole, and T. H. Giddings, “Conventional transmission electron microscopy,” *Mol. Biol. Cell*, vol. 25, no. 3, pp. 319–323, 2014.

[64] R. Shukla, V. Bansal, M. Chaudhary, A. Basu, R. R. Bhonde, and M. Sastry, “Biocompatibility of gold nanoparticles and their endocytotic fate inside the cellular compartment: A microscopic overview,” *Langmuir*, vol. 21, no. 23, pp. 10644–10654, 2005.

[65] S. Rakoff-Nahoum, “Why cancer and inflammation?,” *Yale J. Biol. Med.*, vol. 79, no. 3–4, pp. 123–130, 2006.

[66] D. J. M, “The effect of particle design on cellular internalization pathways,” *Proc. Natl. Acad. Sci. U. S. A.*, vol. 105, no. 33, p. 11613, 2008.

[67] T. L. Riss *et al.*, “Cell Viability Assays,” in *Assay Guidance Manual*, Bethesda (MD): Eli Lilly & Company and the National Center for Advancing Translational Sciences, 2016, pp. 357–

388.

[68] L. Fuentes *et al.*, “HHS Public Access,” vol. 93, no. 4, pp. 292–297, 2016.

[69] E. Vega-Avila and M. K. Pugsley, “An Overview of Colorimetric Assay Methods Used to Assess Survival or Proliferation of Mammalian Cells,” *Proc . West . Pharmacol . Soc*, vol. 54, no. January, pp. 10–14, 2011.

[70] X. Feng Wang, A. Periasamy, B. Herman, and D. M. Coleman, “Fluorescence Lifetime Imaging Microscopy (FLIM): Instrumentation and Applications,” *Crit. Rev. Anal. Chem.*, vol. 23, no. 5, pp. 369–395, 1992.

[71] M. Wahl, “Time-correlated single photon counting,” pp. 1–14, 2014.

[72] W. Becker, “Fluorescence lifetime imaging - techniques and applications,” *J. Microsc.*, vol. 247, no. 2, pp. 119–136, 2012.

[73] E. Zelazny, J. W. Borst, M. Muylaert, H. Batoko, M. A. Hemminga, and F. Chaumont, “FRET imaging in living maize cells reveals that plasma membrane aquaporins interact to regulate their subcellular localization,” *Proc. Natl. Acad. Sci.*, vol. 104, no. 30, pp. 12359–12364, 2007.

[74] S. E. D. Webb *et al.*, “Single-molecule imaging and fluorescence lifetime imaging microscopy show different structures for high- and low-affinity epidermal growth factor receptors in A431 cells,” *Biophys. J.*, vol. 94, no. 3, pp. 803–819, 2008.

[75] E. Russinova, “Heterodimerization and Endocytosis of Arabidopsis Brassinosteroid Receptors BRI1 and AtSERK3 (BAK1),” *Plant Cell Online*, vol. 16, no. 12, pp. 3216–3229, 2004.

[76] C. Vinegoni, P. F. Feruglio, I. Gryczynski, R. Mazitschek, and R. Weissleder, “Fluorescence anisotropy imaging in drug discovery,” *Adv. Drug Deliv. Rev.*, 2018.

[77] D. M. Jameson, “Fluorescence Polarisation/Anisotropy in Diagnostics and Imaging,” *Burns*, vol. 110, no. 5, pp. 2685–2708, 2011.

[78] M. Tramier and M. Coppey-Moisan, “Fluorescence Anisotropy Imaging Microscopy for Homo-FRET in Living Cells,” *Methods Cell Biol.*, vol. 85, no. 08, pp. 395–414, 2008.

[79] H. D. Vishwasrao, P. Trifilieff, and E. R. Kandel, “In vivo imaging of the actin polymerization state with two-photon fluorescence anisotropy,” *Biophys. J.*, vol. 102, no. 5, pp. 1204–1214, 2012.

[80] B. P. Lucey, W. A. Nelson-Rees, and G. M. Hutchins, “Historical Perspective Henrietta Lacks, HeLa Cells, and Cell Culture Contamination,” *Arch Pathol Lab Med*, vol. 133, no. 9,

pp. 1463–1467, 2009.

[81] Y. Chao and T. Zhang, "Optimization of fixation methods for observation of bacterial cell morphology and surface ultrastructures by atomic force microscopy," *Appl. Microbiol. Biotechnol.*, vol. 92, no. 2, pp. 381–392, 2011.

[82] S. Yokota and Y. Okada, "Effect of Fixation with Reduced Osmium Tetroxide upon the Antigenicity of Liver Catalase and Erythrocyte Esterase D," *Acta Histochem. Cytochem.*, vol. 29, no. 4, pp. 335–338, 1996.

[83] A. Kasten, C. Grüttner, J. P. Kühn, R. Bader, J. Pasold, and B. Frerich, "Comparative in vitro study on magnetic iron oxide nanoparticles for mri tracking of adipose tissue-derived progenitor cells," *PLoS One*, vol. 9, no. 9, 2014.

[84] K. R. Wierzbinski *et al.*, "Potential use of superparamagnetic iron oxide nanoparticles for in vitro and in vivo bioimaging of human myoblasts," *Sci. Rep.*, vol. 8, no. 1, pp. 1–17, 2018.

[85] Y. Liu, Z. Chen, and J. Wang, "Systematic evaluation of biocompatibility of magnetic Fe3O4 nanoparticles with six different mammalian cell lines," *J. Nanoparticle Res.*, vol. 13, no. 1, pp. 199–212, 2011.

[86] ISO 10993-5:2009, "Biological evaluation of medical devices – Part 5: Tests for in vitro cytotoxicity," 2009.

[87] S. M. Borisov and O. S. Wolfbeis, "Temperature-sensitive europium(III) probes and their use for simultaneous luminescent sensing of temperature and oxygen," *Anal. Chem.*, vol. 78, no. 14, pp. 5094–5101, 2006.

[88] Roberto Dominguez and Kenneth C. Holmes, "NIH Public Access," *Annu Rev Biophys. 2011 Jube 9; 40 169-186.doi10.1146/annurev-biophys-042910-155359*, no. 3, pp. 169–186, 2011.

[89] H. Lodish, A. Berk, S. L. Zipursky, D. Baltimore, and J. Darnell, "Section 18.1 The Actin Cytoskeleton," in *Molecular Cell Biology*, 4th ed., New York: W. H. Freeman, 2000.

[90] T. C. Vessoni Penna, M. Ishii, O. Cholewa, and L. C. De Souza, "Thermal characteristics of recombinant green fluorescent protein (GFPuv) extracted from Escherichia coli," *Lett. Appl. Microbiol.*, vol. 38, no. 2, pp. 135–139, 2004.

[91] A. N. Bader, E. G. Hofman, J. Voortman, P. M. P. Van Bergen En Henegouwen, and H. C. Gerritsen, "Homo-FRET imaging enables quantification of protein cluster sizes with subcellular resolution," *Biophys. J.*, vol. 97, no. 9, pp. 2613–2622, 2009.

[92] N. Lane and W. Martin, "The energetics of genome complexity," *Nature*, vol. 467, no. 7318,

pp. 929–934, 2010.

[93] “CellLight Mitochondria-GFP, BacMam 2.0 - Thermo Fisher Scientific.” [Online]. Available: https://www.thermofisher.com/order/catalog/product/C10600. [Accessed: 19-Sep-2018].

[94] D. Chrétien *et al.*, “Mitochondria are physiologically maintained at close to 50 °C,” *PLoS Biol.*, vol. 16, no. 1, pp. 1–17, 2018.

[95] S. Kiyonaka *et al.*, “Genetically encoded fluorescent thermosensors visualize subcellular thermoregulation in living cells,” *Nat. Methods*, vol. 10, no. 12, pp. 1232–1238, 2013.

[96] S. T. Smiley *et al.*, “Intracellular heterogeneity in mitochondrial membrane potentials revealed by a J-aggregate-forming lipophilic cation JC-1.,” *Proc. Natl. Acad. Sci.*, vol. 88, no. 9, pp. 3671–3675, 1991.

[97] T. Bai and N. Gu, “Micro/Nanoscale Thermometry for Cellular Thermal Sensing,” *Small*, vol. 12, no. 34, pp. 4590–4610, 2016.

[98] S. Arai, S. C. Lee, D. Zhai, M. Suzuki, and Y. T. Chang, “A molecular fluorescent probe for targeted visualization of temperature at the endoplasmic reticulum,” *Sci. Rep.*, vol. 4, 2014.

[99] S. Arai *et al.*, “Mitochondria-targeted fluorescent thermometer monitors intracellular temperature gradient†,” *Chem. Commun.*, vol. 51, no. 8044, pp. 8044–8047, 2015.

[100] M. Homma, Y. Takei, A. Murata, T. Inoue, and S. Takeoka, “A ratiometric fluorescent molecular probe for visualization of mitochondrial temperature in living cells,” *Chem. Commun.*, vol. 51, no. 28, pp. 6194–6197, 2015.

[101] L. Yang, H. S. Peng, H. Ding, F. T. You, L. L. Hou, and F. Teng, “Luminescent Ru(bpy)32+-doped silica nanoparticles for imaging of intracellular temperature,” *Microchim. Acta*, vol. 181, no. 7–8, pp. 743–749, 2014.

[102] J. Dong and J. I. Zink, “Taking the temperature of the interiors of magnetically heated nanoparticles,” *ACS Nano*, vol. 8, no. 5, pp. 5199–5207, 2014.